




BMP3 is a novel locus involved in the causality of ocular coloboma

Sabrina C. Fox^{1,3} · Sonya A. Widen^{1,2,3} · Mika Asai-Coakwell^{4,7} · Serhiy Havrylov^{6,7} · Matthew Benson^{6,7} · Lisa B. Prichard⁵ · Pranidhi Baddam⁸ · Daniel Graf^{6,8} · Ordan J. Lehmann^{3,6,7} · Andrew J. Waskiewicz^{1,3} 

Received: 3 September 2021 / Accepted: 4 January 2022

© The Author(s), under exclusive licence to Springer-Verlag GmbH Germany, part of Springer Nature 2022

Abstract

Coloboma, a congenital disorder characterized by gaps in ocular tissues, is caused when the choroid fissure fails to close during embryonic development. Several loci have been associated with coloboma, but these represent less than 40% of those that are involved with this disease. Here, we describe a novel coloboma-causing locus, *BMP3*. Whole exome sequencing and Sanger sequencing of patients with coloboma identified three variants in *BMP3*, two of which are predicted to be disease causing. Consistent with this, *bmp3* mutant zebrafish have aberrant fissure closure. *bmp3* is expressed in the ventral head mesenchyme and regulates phosphorylated Smad3 in a population of cells adjacent to the choroid fissure. Furthermore, mutations in *bmp3* sensitize embryos to Smad3 inhibitor treatment resulting in open choroid fissures. Micro CT scans and Alcian blue staining of zebrafish demonstrate that mutations in *bmp3* cause midface hypoplasia, suggesting that *bmp3* regulates cranial neural crest cells. Consistent with this, we see active Smad3 in a population of periocular neural crest cells, and *bmp3* mutant zebrafish have reduced neural crest cells in the choroid fissure. Taken together, these data suggest that Bmp3 controls Smad3 phosphorylation in neural crest cells to regulate early craniofacial and ocular development.

Sabrina C. Fox and Sonya A. Widen contributed equally to this work.

✉ Andrew J. Waskiewicz
aw@ualberta.ca

¹ Department of Biological Sciences, University of Alberta, 11455 Saskatchewan Drive, Edmonton, AB T6G 2E9, Canada

² Vienna BioCenter, Institute of Molecular Biotechnology of the Austrian Academy of Sciences (IMBA), Vienna, Austria

³ Women and Children's Health Research Institute, University of Alberta, Edmonton, AB, Canada

⁴ Department of Animal and Poultry and Animal Science, University of Saskatchewan, Saskatoon, SK, Canada

⁵ Department of Biological Sciences, MacEwan University, Edmonton, AB, Canada

⁶ Department of Medical Genetics, University of Alberta, Edmonton, AB, Canada

⁷ Department of Ophthalmology, University of Alberta, Edmonton, AB, Canada

⁸ Department of Dentistry, University of Alberta, Edmonton, AB, Canada

Introduction

Vertebrate ocular development is a deeply conserved and highly coordinated developmental process. As such, even minor perturbations can lead to ocular malformations which, in many cases, are blinding. During gastrulation, retinal tissues in the eye field evaginate to form bilateral optic vesicles (Zuber et al. 2003). These vesicles migrate laterally until they contact the overlying ectoderm and induce lens formation. Subsequent coordinated invagination of the vesicles forms the bi-layered structure of the optic cup, with the lens-facing layer forming the neural retina and the lens-averted layer becoming the retinal pigmented epithelium (Schmitt and Dowling 1994; Kagiya et al. 2005; Kwan et al. 2012). During optic cup invagination, a transient opening forms on the ventral side of the optic cup known as the optic or choroid fissure (Schmitt and Dowling 1994; Kwan et al. 2012). The choroid fissure acts as a conduit for the early embryonic ocular vasculature and optic nerve, and closure of the choroid fissure is necessary for normal ocular development (Schmitt and Dowling 1994). Failure of choroid fissure closure results in gaps in ocular tissues such as the iris and retina (Shah et al. 2012). In humans, this congenital ocular malformation is referred to as coloboma and is present in 2–19 of

100,000 live births (Williamson and FitzPatrick 2014; ALSomiry et al. 2019; Patel and Sowden 2019; Yoon et al. 2020). Coloboma and its related disorders microphthalmia (reduced ocular size) and anophthalmia (absence of one or both eyes), frequently described as MAC, account for up to 11% of cases of pediatric blindness (Yoon et al. 2020).

Although coloboma can be caused by changes to environmental factors during gestation, it is primarily caused by mutations in genes necessary for ocular development (Williamson and FitzPatrick 2014; ALSomiry et al. 2019; Patel and Sowden 2019; Yoon et al. 2020). To date, more than 40 coloboma-causing loci have been identified (ALSomiry et al. 2019; Yoon et al. 2020). These genes have well characterized roles in critical developmental processes essential to choroid fissure closure, including axial patterning of the optic cup (proximal–distal, nasal–temporal and dorsal–ventral), cell movement and shape changes, cell adhesion, extracellular matrix remodeling, and apoptosis (ALSomiry et al. 2019; Yoon et al. 2020). Despite the substantial genetic heterogeneity, the majority of patients with coloboma do not have mutations in any known loci (Yoon et al. 2020). In addition, coloboma exhibits highly variable inheritance, with instances of coloboma pedigrees that display incomplete penetrance and reduced expressivity, suggesting that modifier loci, environmental factors, and stochastic developmental events may confound the identification of disease-causing loci. This is further complicated by marked phenotypic heterogeneity with a diverse spectrum of severity, involvement of distinct ocular structures, and frequent unilateral disease (Morrison et al. 2002; Hornby et al. 2003; Shah et al. 2012; Prokudin et al. 2014).

Of the loci that regulate choroid fissure closure, a significant proportion belong to the Transforming Growth Factor Beta (TGF- β) superfamily of signaling ligands (Williamson and FitzPatrick 2014; ALSomiry et al. 2019; Patel and Sowden 2019; Yoon et al. 2020). All TGF- β superfamily members contain three centralized disulfide bonds termed a “cysteine knot”, as well as an additional disulfide bond that allows for homo- or heterodimerization of ligands (Goebel et al. 2019). This cysteine knot structure and additional disulfide bond are essential for the secretion, stability, and function of these ligands, and loss of this structure severely impairs the activity of these ligands (Goebel et al. 2019). Binding of the extensive family of TGF- β ligand dimers to a smaller cohort of tetrameric complex of Type I and Type II receptors triggers the phosphorylation of receptor-associated Sma- and Mad-related (r-Smad) proteins (Wrana et al. 1992; Bassing et al. 1994; Zhang et al. 1996). Phosphorylated r-Smad recruits co-Smad4, and this complex translocates to the nucleus, where it regulates target gene expression (Liu et al. 1996). TGF- β ligands can be divided into two groups: the Bone Morphogenetic Protein (BMP) subgroup, which typically trigger the phosphorylation of Smad1/5/8, and

the Activin/Nodal/TGF- β subgroup, which predominantly induce the phosphorylation of Smad2/3 (Graff et al. 1996).

Of the two groups of TGF- β ligands, BMPs have been studied most extensively in ocular development and disease. Mutation of BMP pathway members (including ligands, antagonists, co-receptors, receptors and Smads) in patients and/or model organisms contributes to MAC, and mutations in these pathway components are also associated with related phenotypes such as orofacial clefts, craniofacial disorders, and neural tube closure defects (Sakuta et al. 2001; Hanel and Hensey 2006; Morcillo et al. 2006; Asai-Coakwell et al. 2007, 2009; Bakrania et al. 2008; French et al. 2009; Suzuki et al. 2009; Ye et al. 2010; Wyatt et al. 2010; Abouzeid et al. 2011; Reis et al. 2011; Okada et al. 2011; Zhang et al. 2013; Beleggia et al. 2015; Pfirrmann et al. 2015; Yan et al. 2020). BMP ligands are required for ocular cell survival, maintenance of stem cell pools, migration of ocular precursors, and axial patterning of the developing retina (Peters and Cepko 2002; Adler and Belecky-Adams 2002; Morcillo et al. 2006; Asai-Coakwell et al. 2007). Yet, despite intensive investigation, a clear molecular mechanism for how these ligands regulate fissure closure or a plausible explanation for complex patterns of inheritance for genes encoding these pathway components has yet to be deduced.

Early eye development is dependent not only on the intrinsic population of optic cup neuroectoderm cells, but also on a population of extraocular cells that surround the developing eye cup known as the periocular mesenchyme (POM). These cells, which are principally derived from neural crest and cranial mesoderm, migrate over the eye cup and through the choroid fissure and contribute to many structures of the anterior segment, including the iris stroma, the cornea, and components of the intraocular drainage system (Creuzet et al. 2003; Gage et al. 2005; Langenberg et al. 2008). POM cells have also been implicated in choroid fissure closure. Notably, neural crest cells and mesodermally derived endothelial cells are present in the fissure at times that are critical for choroid fissure closure (James et al. 2016; Bernstein et al. 2018; Gestri et al. 2018). Embryos with no appreciable neural crest contribution have open choroid fissures, suggesting that neural crest cells are necessary for closure of the choroid fissure (Gestri et al. 2018; Bryan et al. 2020). Additionally, mutations in transcription factors and signaling molecules associated with neural crest function, including *BMP7*, *ZIC2*, *FOXC1*, *LMX1B*, *ALX1*, and *TFAP2A*, have been shown to cause coloboma, further implicating this population of cells in choroid fissure closure (Morcillo et al. 2006; McMahon et al. 2009; Skarie and Link 2009; Gestri et al. 2009; Lupo et al. 2011; Dee et al. 2012; Sedykh et al. 2017).

Here, we characterize a novel coloboma-causing locus that was identified by exome sequencing a three-generation pedigree of patients with autosomal dominant coloboma and

microphthalmia. Additional variants in *BMP3* were identified in unrelated MAC patients using Sanger sequencing. Use of in-silico predictions and protein secretion assays provided the first evidence that variants have deleterious effects to *BMP3* protein function. Zebrafish CRISPR-generated *bmp3* mutants display both delayed choroid fissure closure and altered jaw development. This prompted us to test the hypothesis that *Bmp3* functions in periocular cells to regulate neural crest cell behavior. We demonstrated that *bmp3* mutants display marked reduced Smad phosphorylation in periocular neural crest cells. Furthermore, overall migration of periocular neural crest cells is dramatically reduced in *bmp3* mutants. Our data thus provide the first evidence of a contribution of *BMP3* to coloboma and highlight the importance of signaling pathways in regulating the function of periocular neural crest during ocular development.

Results

Patients with coloboma and/or microphthalmia have mutations in *BMP3*

To reveal the genetic cause of coloboma in archival samples, we first performed whole exome sequencing (WES) on samples from four individuals affected by autosomal dominant coloboma with accompanying visual deficiencies and one unaffected control individual from a three-generation European pedigree (Fig. 1B). Identified variants were filtered using standard criteria (Fig. 1A) (Beaulieu et al. 2014). Comparison to SNP databases (allele frequency < 1%), in-silico prediction algorithms (MutationTaster, SIFT and PolyPhen), and ocular expression patterns were used to identify rare, potentially damaging variants within genes expressed during ocular morphogenesis (Fig. 1A). This strategy identified 10 variants present in the affected individual's samples (II:2, III:6, III:1, and IV:4) and absent in the unaffected individual's sample (IV:5), of which the point mutation in *BMP3* (c.1408G > C) represented the most promising candidate pathogenic variant (Table 1). Notably, this variant exhibited Mendelian segregation in the larger pedigree, is absent from local control DNA samples, and is absent from the National Heart, Lung and Blood Institute, 1000 Genomes, and gnomAD databases (total of 87,888 exomes and genomes) (Table 2). In addition to this *BMP3* variant, the variant present in *CRYAA* was also an attractive candidate. *CRYAA* encodes Crystallin alpha A, a protein that confers light-focusing properties to the lens (Brady et al. 1997). Mutations in *CRYAA* cause congenital cataracts with high penetrance (Litt et al. 1998; Pras et al. 2000; Mackay et al. 2003; Richter et al. 2008; Laurie et al. 2013). A small number of patients with *CRYAA* mutations and MAC been reported, but most patients with *CRYAA* do not have any

features of MAC (Beby et al. 2007; Sun et al. 2017). Such patients always present with congenital cataracts, and the coloboma present in these patients is predicted to be secondarily caused by defects of the lens (Sun et al. 2017). Since none of the patients in the pedigree from Fig. 1 presented with cataracts, we reasoned that the *CRYAA* variant present in the family from Fig. 1 is likely non-pathogenic. Therefore, the variant in *BMP3* still represents the most plausible variant for causing disease in this family. This mutation alters a residue [p.Ala470Pro (A470P)] that is located between cysteines that mediate the disulfide bonding necessary to form the cysteine knot structure that is essential for TGF- β ligand stability (Fig. S1). This residue is also highly conserved among vertebrate species, further suggesting that it is necessary for the stability and/or function of the mature *BMP3* protein (Fig. S1). Collectively, this strongly indicates that changes to this residue will deleteriously impact protein function. Given that numerous TGF- β superfamily members have essential roles in ocular development and mutations in multiple TGF- β paralogs cause coloboma, we concluded that this *BMP3* variant represented the most plausible pathogenic variant of those identified in this family (Lo et al. 1998; Asai-Coakwell et al. 2007; Bakrania et al. 2008; Ye et al. 2010; Abouzeid et al. 2011).

Additional *BMP3* variants are present in an unrelated cohort of MAC patients.

To determine whether this exceedingly rare mutation indicates that *BMP3* might contribute to coloboma, we searched for additional *BMP3* mutations by conducting Sanger sequencing of *BMP3* in patients unrelated to the pedigree family. DNA samples from a cohort of individuals with microphthalmia, anophthalmia and coloboma phenotypes with accompanying visual deficiencies were collected over the past 20 years through national and international collaboration. Sanger sequencing of 154 samples identified two additional point mutations in *BMP3* that cause single amino acid substitutions in the mature TGF- β domain of the *BMP3* protein [c.1178C > T (p.Ser393Phe) and c.1349 T > A (p.Phe450Tyr)] (Fig. 1C, D). The Ser393Phe variant is present at exceedingly low rates in genome databases (1/76, 069 in gnomAD), whereas the Phe450Tyr variant is present in some control individuals in several databases (1/6732 in NHBLI, 1/5000 in 1 KG, and 29/76, 064 in gnomAD) (Table 2). In-silico modeling using SIFT, PolyPhen2, and MutationTaster predict that the three variants are damaging to protein function, further suggesting that these are pathogenic variants (Table 3). Subsequent use of ANOLEA to bioinformatically predict protein structure indicated that each variant would also increase the free energy required to fold the *BMP3* protein (Fig S2) (Melo et al. 1997). Such predictions, together

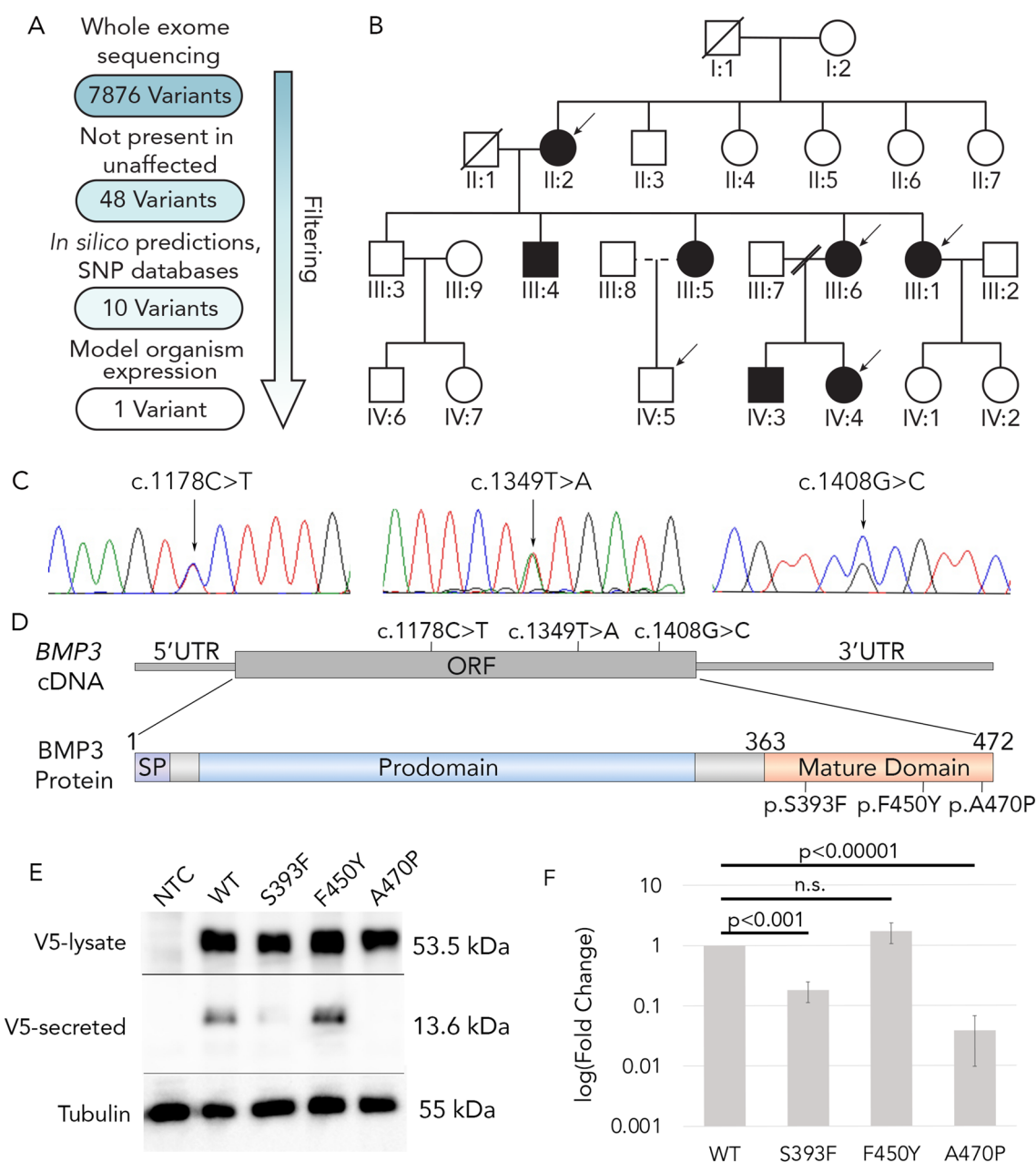


Fig. 1 *BMP3* missense mutations identified in patients with ocular coloboma and microphthalmia. **A** A flow chart outlining the standardized criteria used for filtering human patient variants used in this study. **B** Four-generation pedigree of a family with autosomal dominant coloboma and/or microphthalmia. Whole exome sequencing (WES) was performed on DNA samples from specified individuals (arrows). WES identified a variant in *BMP3* (c.1408G>C), and two additional variants were identified from Sanger sequencing of an independent cohort of unrelated patients (c.1178C>T and c.1349 T>A). **C** Chromatograms showing DNA sequence variants indicated by their base change within the coding sequence of *BMP3*. **D** Schematic of the *BMP3* cDNA and protein, with the position of each nucleotide variant and resulting amino acid substitution indicated. (SP) signal peptide, (ORF) open reading frame. **E** Immunoblots for V5-tagged *BMP3* wildtype and variants. Cos-7 cells were transfected with equal amounts of plasmid DNA encoding V5-tagged *BMP3* proteins, then immunoblots were performed on protein extracted from either the culture media or cell lysates. Immunoblots

performed on cell lysates (top, V5-lysate) show that all *BMP3* proteins are made in approximately equal amounts, but those performed on protein extracted from the culture media (middle, V5-secreted) demonstrate that the S393F and A470P variants, but not F450Y, result in reduced secretion of *BMP3* protein. **F** Quantification of three independent immunoblots. Band intensity for V5-secreted WT, S393F, F450Y, and A470P was measured using ImageJ software and the fold change in intensity for S393F, F450Y, and A470P was calculated relative to WT. Quantification indicates that the fold change in band intensity for V5-secreted S393F (0.180 ± 0.0670 -fold change) and A470P (0.0384 ± 0.0285 -fold change) are significantly reduced compared to wildtype (Student's *t* test, $t_2 = 12.2$ and 33.7 , $p < 0.0001$ for both). The fold change in band intensity for V5-secreted F450Y variant (1.71 ± 0.645 -fold change) was not significant relative to WT (Student's *t* test, $t_2 = -1.10$, $p = 0.333$). Results are representative of three independent experiments and immunoblots. Error bars represent standard error of the mean (NTC no transfection control, *kDa* kilodaltons, n.s. not statistically significant)

Table 1 A list of candidate genes identified from exome sequencing of patients from a pedigree of autosomal dominant coloboma and microphthalmia

Gene	Amino acid variant	SIFT score	PolyPhen2 score
BMP3	p.Ala470Pro	0	1
VPS72	p.Tyr89Cys	0	0.992
NLRC3	p.Arg51Trp	0	0.998
SARM1	p.Arg230Cys	0	1
SEMA5B	p.Arg273His	0	0.992
PDZD9	p.Glu104*	n/a	n/a
TTC3	p.Pro1239Ser	n/a	0.999
ZNF658	p.Pro657Leu	0	0.999
MYH3	p.Asp1178Asn	0.01	0.994
CRYAA	p.Arg96Cys	0	1

Exome sequencing was conducted on four affected individuals and one unaffected individual. Exome sequencing data were analyzed to only include non-synonymous variants that were not detected in the unaffected control individual or in control exome databases. A SIFT score closer to 0 indicates a variant that is potentially disease-causing, while a PolyPhen2 score closer to 1 indicates a variant that is potentially disease-causing

Table 2 *BMP3* variants identified in this study are found at extremely low frequencies in genome databases

CDS Change	AA Change	Controls	NHLBI	1 KG	gnomAD
c.1178C>T	p.Ser393Phe	0/192	0/6732	0/5000	1/76, 069
c.1349 T>A	p.Phe450Tyr	0/268	1/6732	1/5000	29/76, 064
c.1408G>C	p.Ala470Pro	0/257	0/6732	0/5000	0/76, 156

None of the variants are detected in unaffected control samples. The p.Ala470Pro variant is not detected in any genome databases, while the p.Phe450Tyr and p.Ser393Phe variants are found only at extremely low frequencies in genome databases

CDS coding sequence, AA amino acid, NHLBI National Heart, Lung, and Blood Institute Exome Variant Server, 1 KG 1000 Genomes Project, gnomAD Genome Aggregation Database

with the rarity of the alleles in the general population, suggested that S393F and A470P represented pathogenic variants (Table 3). Since the F450Y allele is present in a larger portion of the general population, it is less likely to represent a disease-causing variant.

Table 3 The *BMP3* variants identified in this study are predicted to be deleterious to protein function

CDS Change	AA Change	SIFT	PolyPhen2	MutationTaster
c.1178C>T	p.Ser393Phe	0.00 (not tolerated)	1.00 (probably damaging)	0.999 (disease causing)
c.1349 T>A	p.Phe450Tyr	0.13 (tolerated)	0.995 (probably damaging)	0.999 (disease causing)
c.1408G>C	p.Ala470Pro	0.00 (not tolerated)	1.00 (probably damaging)	0.999 (disease causing)

All three variants in this study are predicted to be damaging to protein function by SIFT, PolyPhen2, and MutationTaster with the exception of pPhe450Tyr, which is predicted by SIFT to be tolerated

CDS coding sequence, AA amino acid

Functional abnormalities induced by the BMP3 mutations

To determine whether these variants altered the stability and secretion of the BMP3 ligand, the expression of V5-tagged wildtype and variant BMP3 proteins was assayed by immunoblotting. While both wildtype and variant V5-tagged BMP3 were initially expressed in transfected COS cells, differences were observed in the secretion of the BMP3 variants. There was a reduced amount of BMP3-S393F, and the complete absence of BMP3-A470P, from the tissue culture media fraction when compared to wildtype BMP3 (Fig. 1E). In contrast, BMP3-F450Y was still found to be secreted at levels comparable to wildtype BMP3 (Fig. 1E). When quantified and compared to the level of wildtype BMP3 protein in the culture media, the intensity of the bands corresponding to the S393F and A470P variant protein in the culture media exhibited mean fold changes of 0.180 ± 0.0670 and 0.0384 ± 0.0286 , respectively, and were significantly reduced when compared to wildtype (Student's *t* test, $t_4 = 12.2$ and 33.7 , $p = 0.000257$ and < 0.00001 , respectively) (Fig. 1F). Interestingly, the band corresponding to the F450Y variant exhibited a mean fold change of 1.71 ± 0.646 and did not display significantly altered fold change in secretion when compared to wildtype (Student's *t* test, $t_4 = -1.10$, $p = 0.333$) (Fig. 1F). The reduction of S393F and the absence of A470P from the cell culture media suggests that these variants impact the stability of mature protein or the process by which the protein is secreted from cells, whereas the presence of BMP3-F450Y in the culture media suggests that this variant does not affect the stability or secretion of BMP3.

Zebrafish *bmp3* mutants have choroid fissure closure defects

To understand *BMP3*'s role in ocular morphogenesis and choroid fissure closure, we generated zebrafish *bmp3* mutants using CRISPR/Cas9 mutagenesis. The resulting allele, *bmp3*^{ua1020} (hereafter referred to as *bmp3*^{-/-}), contains two in-frame 3 base pair (bp) deletions and a 5 bp deletion (Figure S3A, Fig. 2A). Each 3 bp deletion induces the loss of a single amino acid in the Bmp3 protein, while the 5 bp deletion causes a frameshift mutation that

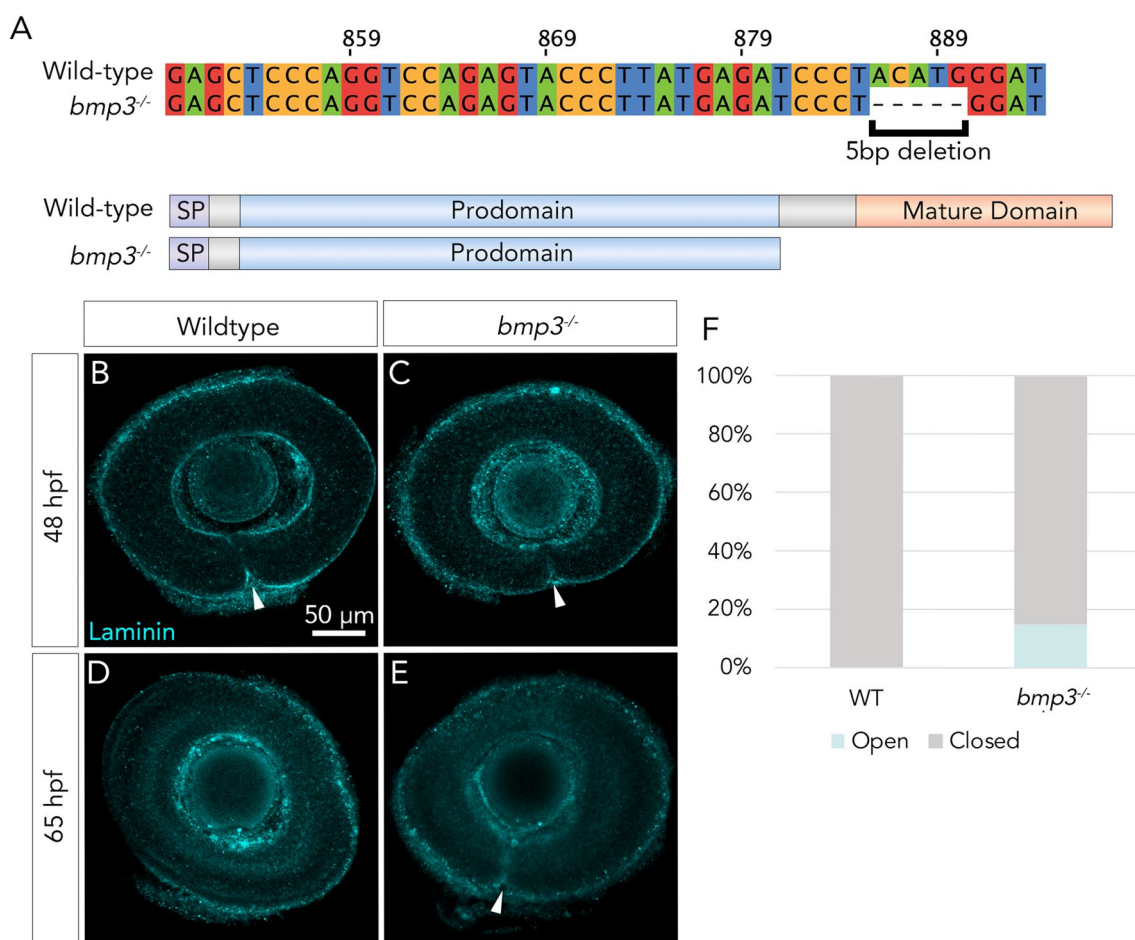


Fig. 2 Zebrafish with mutations in *bmp3* exhibit delayed fissure closure. **A** Partial coding sequence alignment of wildtype and *bmp3*^{ua1020} mutant zebrafish (top) and schematics of each resulting protein (bottom). A 5 bp deletion (c.887_891del) was generated with CRISPR-Cas9, resulting in a frameshift and subsequent premature stop codon (p.Thr96GlyfsTer2). The resulting truncated protein lacks the entire TGF- β mature domain (SP signal peptide). **B–E** Larvae from a *bmp3*^{-/-} heterozygous incross were fixed at 48 or 65 hpf and laminin immunofluorescence was conducted to visualize the extracellular matrix. Eyes were manually dissected and mounted in pairs, then

imaged on a confocal microscope. Both wildtype and *bmp3* mutant larvae at 48 hpf **B, C** show fissure lobes in apposition but incomplete fissure closure (indicated by arrows). In contrast, at 65 hpf **D, E** wildtype larvae have completed fissure closure, while 23/130 *bmp3* mutants show bilateral open fissures (arrowheads). Images were taken at the midpoint of the proximal–distal axis of the optic cup. **F** Quantification of fissure phenotypes in **B–E**, showing 18% bilateral open fissures in *bmp3* mutant larvae at 65 hpf (WT wildtype, *Open* open choroid fissures, *Closed* closed choroid fissures)

introduces a premature stop codon immediately upstream of the sequence encoding the mature TGF- β domain (Fig. S3B). This results in a truncated protein lacking the domain essential for normal BMP function (Fig. 2A), and our analyses revealed no evidence that the mutant transcript undergoes nonsense mediated decay (Fig. S4). Furthermore, the absence of *bmp3* transcript in 2-cell stage embryos suggests that there is no compensatory maternally deposited mRNA (Figure S5). Notably, there are no overt phenotypes present in *bmp3*^{-/-} embryos during the first three days of zebrafish development, nor was there a decrease in survival of *bmp3*^{-/-} mutants from 24 to 72 hpf, suggesting that the role of *bmp3* in early development is subtle (Fig. S6).

The basement membrane surrounding the temporal and nasal retinal lobes, which must be disassembled to allow the lobes to fuse, provides an accurate readout for choroid fissure closure (Hero 1989, 1990; Tsuji et al. 2012; James et al. 2016). Therefore, the absence of the basement membrane lining the fissure is an accurate measure of fissure closure. Loss of this basement membrane is readily visualized with Laminin immunofluorescence. At 48 hpf, the stage just prior to choroid fissure closure, the lobes of both wildtype and mutant choroid fissures are apposed but not yet completely fused (Fig. 2B, C). In contrast, at 65 hpf 18% (23/130) of *bmp3*^{-/-} mutant embryos retained the basement membrane surrounding the fissure compared to 0% (0/38) of wildtype controls demonstrating that *bmp3* contributes

to normal choroid fissure closure (Fig. 2D–F). Statistical analysis (two-sided Fisher's exact test) confirmed that open choroid fissures occur more frequently in *bmp3*^{-/-} mutants when compared to wildtype animals at 65 hpf (Fisher's exact test, $p = 0.0025$). These data also provide evidence that the *bmp3*^{-/-} choroid fissure phenotype is partially penetrant, as is observed in some coloboma pedigrees (Fig. S7).

***bmp3* is expressed in the ventral head mesenchyme surrounding the eye**

To explore the mechanisms by which *bmp3* facilitates choroid fissure closure, the spatial expression of *bmp3* mRNA was assessed. The earliest localized cranial expression

of *bmp3* begins at approximately 22 hpf, with dorsal flat mounts demonstrating *bmp3* is expressed in the vicinity of the forebrain and the eye (Fig. 3A). Cranial coronal sections reveal that *bmp3* is expressed in a single-cell thick layer in the head mesenchyme immediately ventral to the eye (Fig. 3B). Transverse sections of the head further confirm *bmp3* expression in the head mesenchyme between the brain and retina and not within the neuroepithelial cells of the retina or brain (Fig. 3C and D). In conclusion, *bmp3* is expressed in the ventral head mesenchyme adjacent to the choroid fissure.

During ocular development, periocular neural crest cells originating from the diencephalon and anterior midbrain migrate to the posterior aspect of the developing eye vesicle

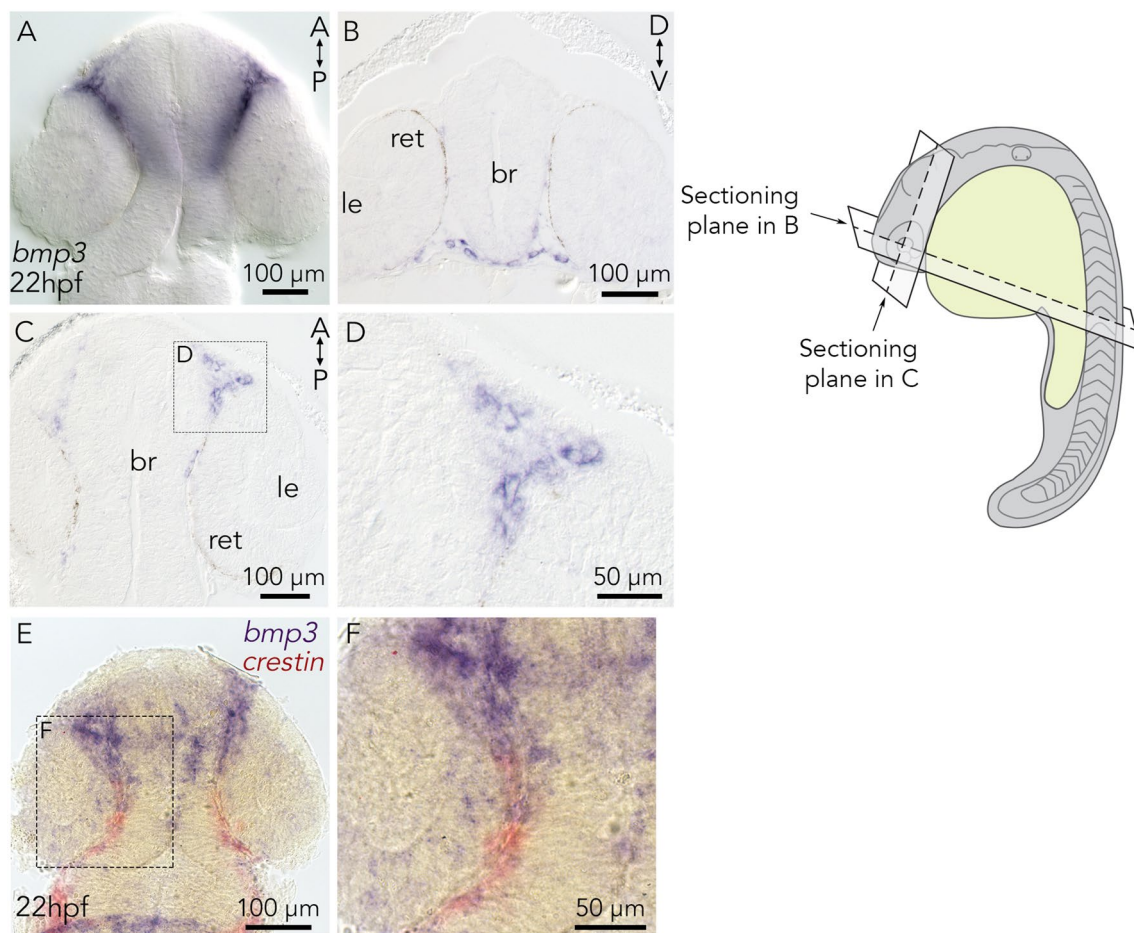


Fig. 3 *bmp3* is expressed in the periocular mesenchyme during ocular morphogenesis. Whole mount in situ hybridization was conducted on wildtype embryos to assess the localization of *bmp3* mRNA during early ocular morphogenesis. **A** Dorsal view of dissected and flat mounted embryo at 22 hpf. *bmp3* expression is localized head mesenchyme between the retina and the forebrain. **B–D** Embryos were embedded in paraffin wax after in situ hybridization, then sectioned and mounted on slides. Coronal sections through the middle of the optic cup **B** show *bmp3* expression in a single cell-thick layer in the head mesenchyme directly ventral to the eye. Transverse sections

C, D show that *bmp3* transcript is specifically expressed in the head mesenchyme between the forebrain and the retina. The box in **C** indicates the area magnified in **D**. **E, F** Two-color *in-situ* hybridization using probes for *bmp3* (purple) and *crestin* (red) at 22 hpf. *bmp3* is expressed just anteriorly to *crestin* at 22 hpf, suggesting that *bmp3* may regulate *crestin*-expressing neural crest cells as they migrate over the anterior portion of the eye prior to entry into the choroid fissure. The box in **E** indicates the area magnified in **F** (A anterior, P posterior, D dorsal, V ventral, le lens, br brain, ret retina)

between 14 and 18 hpf (Langenberg et al. 2008). From 18 to 24 hpf, these cells migrate over the anterior and lateral surface of the eye, contributing to many structures of the anterior segment (Langenberg et al. 2008). To ascertain whether *bmp3* is expressed in or near periocular neural crest cells, two-color *in-situ* hybridization was conducted on 22 hpf embryos using probes for *bmp3* and *crestin*, a transcript expressed exclusively in neural crest cells (Luo et al. 2001). At this stage, *crestin*-expressing cells are localized to the posterior portion of the eye, whereas *bmp3* transcript is localized to cells in the anterior portion of the eye (Fig. 3E, F), suggesting that *bmp3* may be a potential regulator of periocular neural crest cells as they migrate over the anterior portion of the eye. In conclusion, *bmp3* expression is positioned optimally to regulate neural crest cells as they migrate through the periocular region.

Bmp3 does not regulate dorsal–ventral patterning of the early eye

During ocular morphogenesis, the eye must be patterned along the dorsal–ventral axis (Peters and Cepko 2002). This is achieved through opposing gradients of dorsally restricted targets of BMP signaling and ventrally restricted targets of Sonic Hedgehog signaling (Peters and Cepko 2002). To determine whether *bmp3* facilitates dorsal–ventral axis patterning of the optic cup, the spatial expression of genes that are restricted to either the dorsal (*tbx5a*, *aldh1a2*) or the ventral (*vax2*, *aldh1a3*) regions of the eye were examined in wildtype and *bmp3*^{−/−} mutants using *in-situ* hybridization (Peters and Cepko 2002). In wildtype embryos, the expression of dorsal markers is restricted to the dorsal half of the optic cup, and ventral markers are restricted to the ventral optic cup, as expected (*n* = 25) (Fig. 4A, C, E, G). Identical expression patterns are observed in *bmp3*^{−/−} mutants (*n* = 25) (Fig. 4B, D, F, H), suggesting that *bmp3* does not regulate axial patterning of the retina.

Bmp3 does not regulate proliferation or apoptosis in the early eye

In addition to dorsal–ventral patterning of the optic cup, aberrancies in optic cup cell proliferation have also previously been shown to contribute to the appearance of a coloboma phenotype in several animal models (Kim et al. 2007; Viringipurampeer et al. 2012; Lee et al. 2013; Van Nostrand et al. 2014; Noh et al. 2016; Sghari and Gunhaga 2018). Therefore, it is plausible that *bmp3* regulates proliferation or apoptosis of neuroectodermal optic cup cells, and the loss of *bmp3* results in aberrant proliferation or apoptosis, thereby leading to choroid fissure closure defects. To determine whether *bmp3* regulates cell proliferation, immunofluorescence was conducted on 28 hpf wildtype and

bmp3^{−/−} embryos using primary antibodies against phosphorylated Histone H3. We do not observe an obvious change in proliferation of the optic cup in *bmp3*^{−/−} mutants (*n* = 20) when compared to wildtype controls (*n* = 20) (Fig. 4I, J), indicating that *bmp3* likely does not regulate proliferation of the optic cup. Likewise, there is no obvious change in apoptosis of the optic cup between *bmp3*^{−/−} mutants (*n* = 19) when compared to wildtype controls (*n* = 19), as revealed by cleaved Caspase-3 immunofluorescence (Figure S8), indicating that *bmp3* does not regulate apoptosis of cells in the optic cup. Taken together, these results indicate that *bmp3* does not regulate division or death of the neural retina.

Bmp3 facilitates choroid fissure closure via Smad3 phosphorylation

The majority of BMP ligands signal via the phosphorylation of Smad1/5/8 rather than Smad2/3 phosphorylation, which is typical of other TGF- β family members such as Activin and Nodal (Miyazono et al. 2000). Interestingly, BMP3 has been shown to activate Smad2/3 rather than Smad1/5/8, suggesting it functions in a noncanonical manner compared to other BMP ligands (Bahamonde and Lyons 2001; Daluiski et al. 2001; Stewart et al. 2010). To determine the level of Smad3 phosphorylation adjacent to the choroid fissure, immunofluorescence using an anti-phosphorylated Smad3 (pSmad3) primary antibody was first assessed in wildtype embryos. Confocal imaging revealed active phosphorylated Smad3 restricted to cells in the proximal portion of the nasal lobe, adjacent to the choroid fissure (Fig. 5A). In contrast, z-stacks from the medial to distal regions of the eye demonstrated little detectable pSmad3 (Fig. 5B, C). In conclusion, pSmad3 is present in cells that are positioned optimally to facilitate fissure closure.

We next assessed the presence of pSmad3 in wildtype and *bmp3*^{−/−} embryos to determine whether Bmp3 facilitates choroid fissure closure via Smad3 phosphorylation. While the distinct population of pSmad3 positive cells adjacent to the choroid fissure are present in both wildtype and *bmp3*^{−/−} embryos (Fig. 5D, E), there was a subtle, yet statistically significant, reduction in the number of cells containing phosphorylated Smad3 in the ventro-proximal retina of *bmp3*^{−/−} mutants (18.3 ± 1.09 cells) when compared to wildtype siblings (22.2 ± 1.12 cells) (Student's *t* test, $t_{38} = 2.49$, $p = 0.0172$) (Fig. 5F). Since compensation by other TGF- β ligands represents one explanation for the subtlety of the pSmad3 phenotype, we treated *bmp3*^{−/−} mutants with the pharmacological agent Specific Inhibitor of Smad3 (SIS3) and measured choroid fissure closure. SIS3 was titrated to yield an incompletely penetrant phenotype, and the suboptimal dose selected (12 μ M SIS3) yielded open choroid fissures in 15–20% of wildtype embryos. SIS3 treatment from 24–30 hpf resulted in a significantly higher

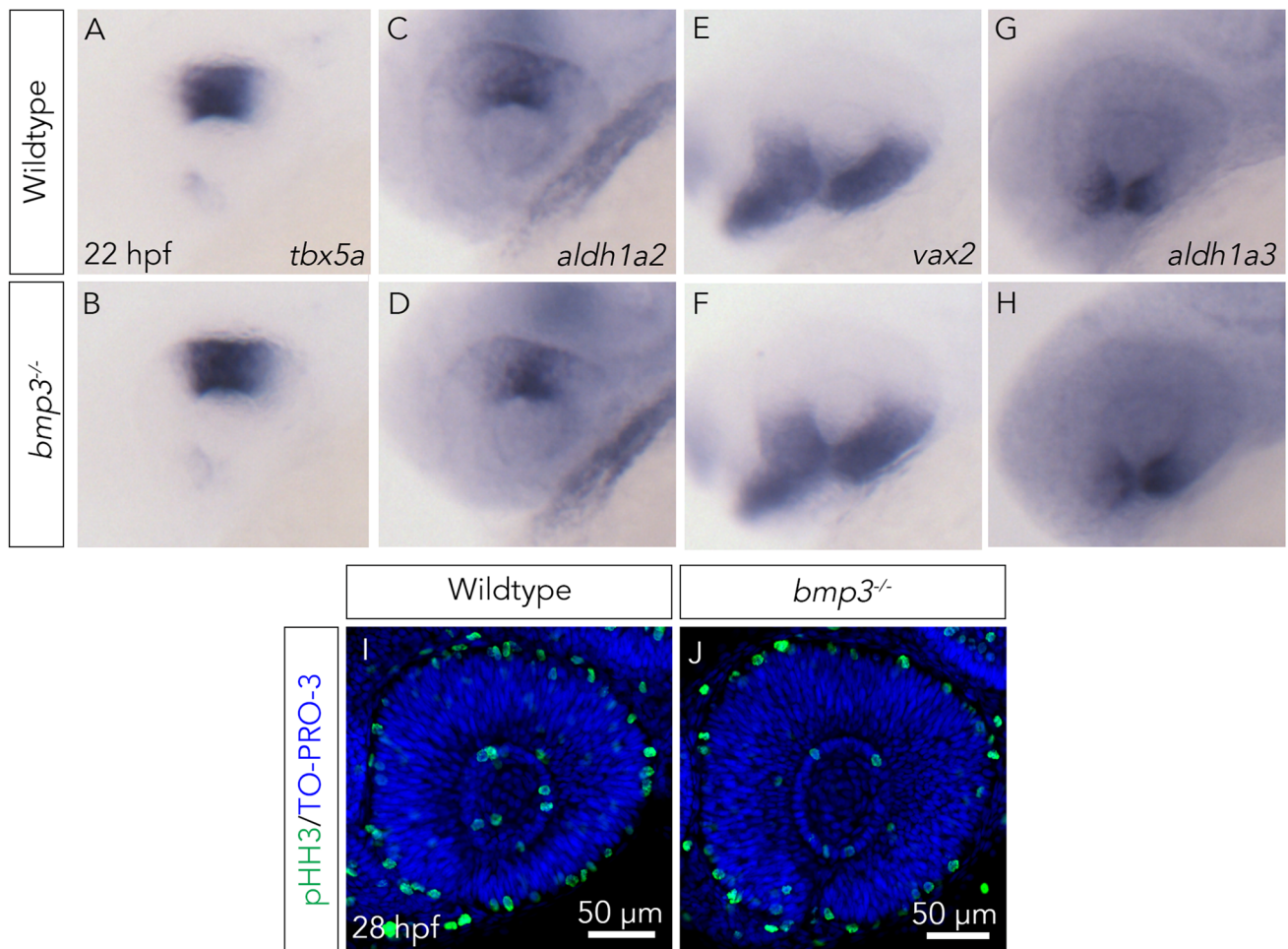


Fig. 4 *bmp3* does not regulate dorsal–ventral patterning or cell proliferation of the optic cup. **A–H** To assess dorsal–ventral patterning of the optic cup in wildtype and *bmp3* mutants, whole mount in situ hybridization was conducted on 22 hpf embryos from a *bmp3*^{+/+} incross, using probes for transcripts that provide a readout of dorsal (*tbx5a*, *aldh1a2*; **A–D**) and ventral (*vax2*, *aldh1a3*; **E–H**) optic cup identity. The expression of dorsal and ventral genes in *bmp3*^{-/-} mutants (**B, D, F** and **H**) is comparable in both intensity and domain to wildtype embryos (**A, C, E** and **G**). Embryos were imaged later-

ally in 3% methylcellulose on a dissecting microscope then used for genomic DNA extraction and genotyping ($n=25$ /probe-genotype combination). **I, J** To assess proliferation and apoptosis of the optic cup in wildtype and *bmp3* mutants, phosphorylated Histone H3 immunofluorescence was conducted on wildtype and *bmp3*^{-/-} mutant embryos at 28hpf. There is no observable difference in proliferation between wildtype (**I**) and *bmp3*^{-/-} mutant (**J**) embryos ($n=20$ /genotype). Images were taken of the at the midpoint of the proximal–distal axis of the optic cup (*pHH3* phospho-Histone H3)

proportion of open choroid fissures in *bmp3*^{-/-} mutants compared to wildtype embryos (*bmp3*^{-/-} 23/31 (74%), WT 5/28 (18%), two proportion z test, $z = -4.33$, $p < 0.00001$, Fig. 5G–I). In summary, these data show that *bmp3* mutations synergize with pharmacological inhibition of Smad3 to impede choroid fissure closure.

Smad3 phosphorylation is active in neural crest cells in the choroid fissure

POM cells are derived from neural crest cells and cranial mesoderm and have previously been shown to be necessary for choroid fissure closure (James et al. 2016; Gestri et al. 2018; Bryan et al. 2020). In a study of canine

brachycephaly, the loss of *BMP3/bmp3* during development results in craniofacial phenotypes including the loss or hypoplasia of early craniofacial cartilage in certain dog breeds and morphant zebrafish (Schoenebeck et al. 2012). This is consistent with our own observations of adult *bmp3*^{-/-} mutants. Midfacial hypoplasia is present in 18-month-old adult *bmp3*^{-/-} zebrafish and is visible under a dissecting microscope (Fig. 6A, B). This is further confirmed by Micro-Computerized Tomography (Micro-CT) scans of adult wildtype and *bmp3*^{-/-} mutants; *bmp3*^{-/-} mutants ($n=5$) have visually altered craniofacial anatomy when compared to wildtype siblings ($n=5$) (Fig. 6C–F). When quantified, *bmp3*^{-/-} mutants display significantly shortened average premaxilla

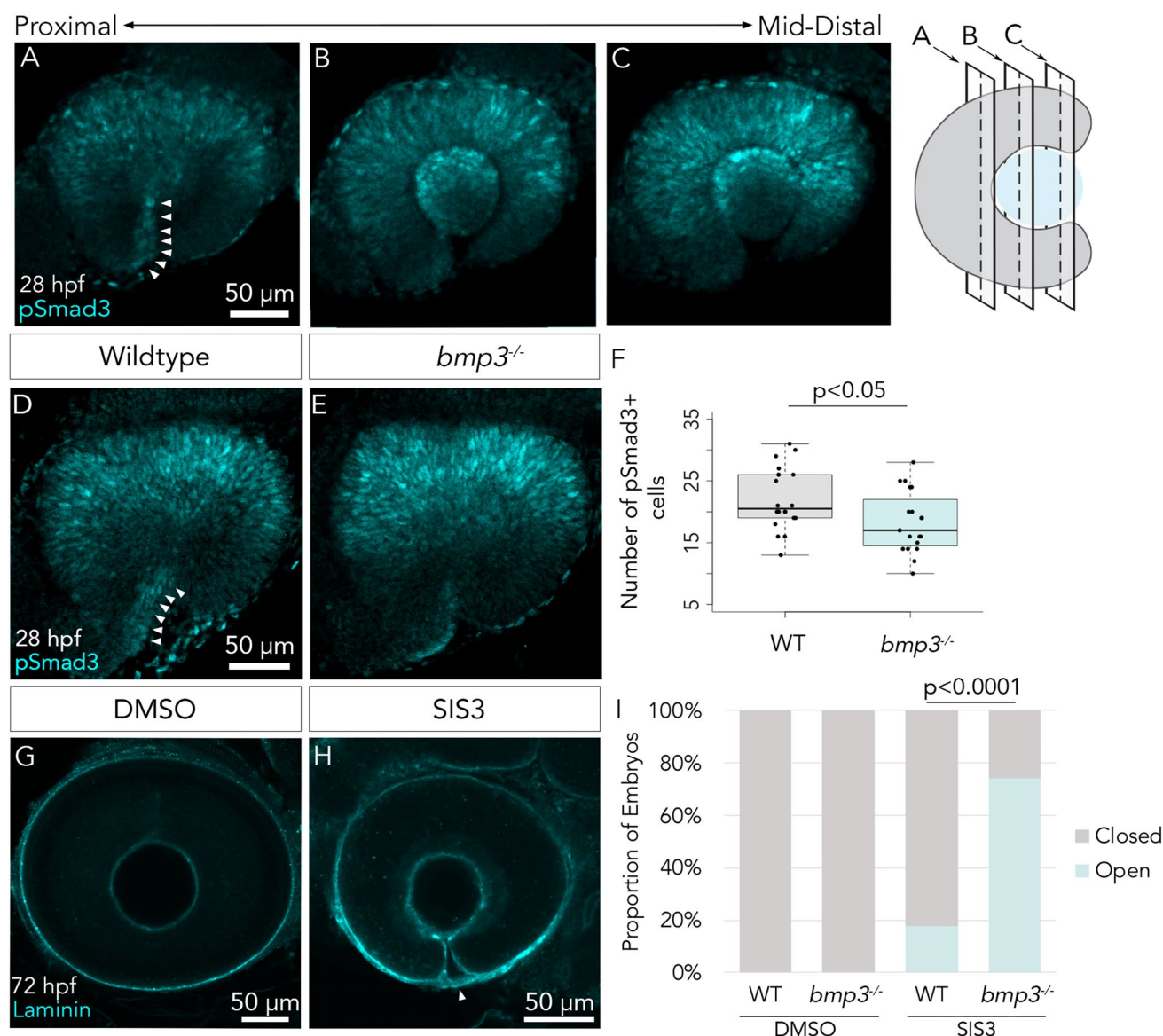


Fig. 5 Smad3 phosphorylation is necessary for choroid fissure closure. **A–C** pSmad3 immunofluorescence conducted on wildtype 28 hpf embryos indicates that TGF- β signaling is active in the nasal lobe of the proximal-ventral eye cup (**A**, arrowheads) but is largely absent in more distal regions of the choroid fissure (**B**, **C**). Schematic diagram (right) indicates the points along the proximal–distal axis of the optic cup that images in **A–C** were acquired **D**, **E** To assess Smad3 phosphorylation in *bmp3* mutants, pSmad3 immunofluorescence was conducted on *bmp3* mutants (**E**) and wildtype siblings **D** at 28 hpf. The number of pSmad3+ cells is reduced in a *bmp3* mutants when compared to wildtype siblings (arrowheads, quantified in **F**). Images were taken of the proximal optic cup immediately posterior to the lens. **F** When quantified, there is a significant decrease in the number of pSmad3+ cells in *bmp3* mutants (18.3 ± 1.09 cells) when

compared to wildtype (22.2 ± 1.12 cells) (Student's *t* test, $t_{38}=2.49$, $p=0.0172$) **G**, **H** Representative images of wildtype embryos treated with a suboptimal dose (12 μ M) of SIS3 from 24–30 hpf. The presence of open choroid fissures was assessed using laminin immunofluorescence. Wildtype embryos display open choroid fissures when treated with SIS3 (**H**, arrowhead), compared to embryos treated with vehicle (DMSO) alone (**G**). Images were taken of the at the midpoint of the proximal–distal axis of the optic cup. **I** A significantly higher proportion of *bmp3*^{-/-} mutant embryos have open choroid fissures compared to wildtype when treated with SIS3 (two-proportion *z* test, $z=-4.32$, $p<0.0001$), suggesting that Bmp3 and Smad3 function in the same pathway. Results are representative of three independent experiments (WT Wildtype, Open open choroid fissure, Closed closed choroid fissure)

(1.20 ± 0.167 mm), maxilla (1.58 ± 0.0676 mm), and mandible (2.23 ± 0.112 mm) length when compared to wildtype siblings (1.58 ± 0.250 mm, 1.88 ± 0.0823 , and 2.68 ± 0.146 mm, respectively) (two sample *t* test,

$t_8=2.85$, 6.22 , and 5.50 , $p=0.000255$, 0.0214 , and 0.000573) (Fig. 6G–I). Additionally, analysis of 7 dpf larval zebrafish jaws stained with Alcian blue revealed that 40% ($n=8/20$) of *bmp3*^{-/-} embryos display jaws that are

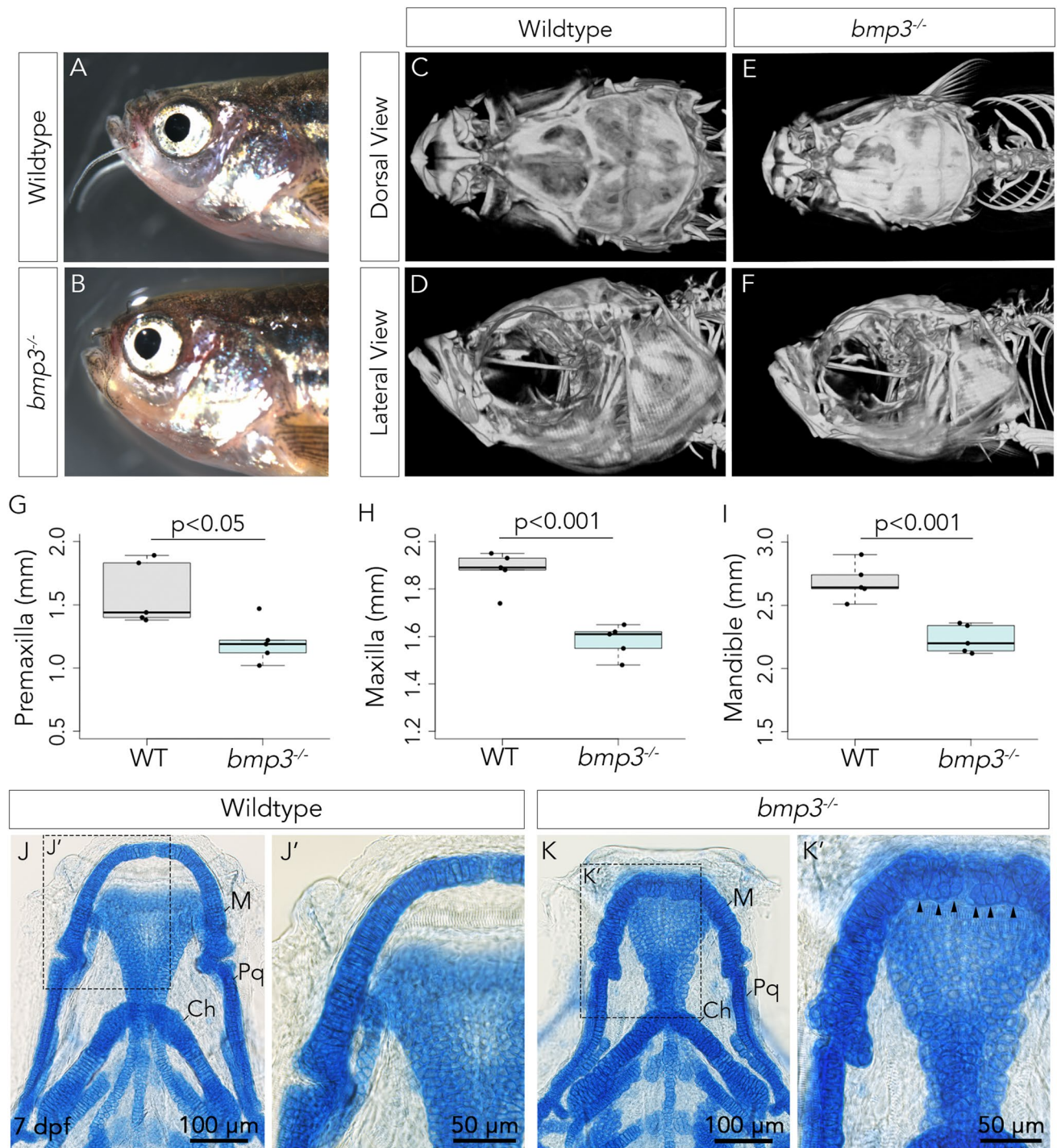


Fig. 6 *bmp3*^{-/-} mutants have midface hypoplasia. Dissecting microscope images (A, B) and micro-CT analysis (C–F) of 18-month-old wildtype (A, C, D) and *bmp3*^{-/-} (B, E, F) zebrafish demonstrate significantly shorter premaxilla (G), maxilla (H) and mandible (I) in the mutant fish ($n=5$) when compared to wildtype siblings ($n=5$) (Student's t test, $t_8=2.85$, 6.22 , and 5.50 , $p=0.000255$, 0.0214 , and 0.000573 , respectively) (WT wildtype). J, K') Alcian blue staining of craniofacial cartilage in 7 dpf larvae indicates that 40% (8/20) of

bmp3^{-/-} mutants (K) have disrupted jaw cartilage formation when compared to wildtype (J) larvae (0/20). The overall anatomy of Meckel's cartilage, the palatoquadrate, and the ceratohyal (J and K) as well as chondrocyte organization and morphology (J', K', arrowheads) are abnormal in a subset of mutants ($n=8/20$) when compared to wildtype controls ($n=0/20$). The boxes in J and K indicate the magnified regions in J' and K', respectively. (M Meckel's cartilage, Pq palatoquadrate, Ch ceratohyal)

hypoplastic when compared to wildtype controls ($n=0/20$) (Fig. 6J, K). The morphology of the chondrocytes that make up Meckel's cartilage are also severely compromised in *bmp3*^{-/-} mutants; the chondrocytes of Meckel's cartilage in affected *bmp3*^{-/-} mutants appear rounder, undifferentiated, and less organized when compared to Meckel's cartilage from wildtype animals, where the chondrocytes are elongated, stacked, and columnar (Fig. 6J', K'). This evidence implicates *bmp3* as a regulator of craniofacial development. Since all craniofacial cartilage and bone is derived from neural crest cells, and since there is no change in patterning, proliferation, apoptosis, and size of the optic cup in *bmp3*^{-/-} mutants, we hypothesize that *bmp3* regulates neural crest cell-mediated choroid fissure closure.

To determine whether pSmad3 is present in cells in the vicinity of periocular neural crest cells, we performed pSmad3 immunofluorescence on *Tg(sox10:EGFP)* embryos, a strain that specifically labels migratory neural crest cells. It has previously been shown that periocular neural crest cells are readily apparent in the choroid fissure at 28–30 hpf (James et al. 2016; Bernstein et al. 2018; Gestri et al. 2018). Therefore, to assess the state of phosphorylated Smad3 in the context of neural crest cells, pSmad3 immunofluorescence was conducted on wildtype *Tg(sox10:EGFP)* embryos at 24, 28, and 32 hpf. We observe neural crest cells near the choroid fissure and in the choroid fissure itself at 24, 28, and 32 hpf (Fig. 7A, D and G). At 24 hpf, neural crest cells have initiated infiltration of the choroid fissure (Fig. 7A). At this time, there is no observable retinal pSmad3 in the proximal retina, suggesting that Smad3 phosphorylation is initiated in the retina after 24 hpf (Fig. 7B). Since there is no colocalization between GFP + neural crest cells and pSmad3 signal, it is unlikely that TGF- β signaling is regulating neural crest cells at this stage (Fig. 7C, C'). At 28 hpf, the choroid fissure and ventral eye have become highly infiltrated with neural crest cells, and within the choroid fissure neural crest cells appear to completely wrap around both lobes of the choroid fissure, namely the nasal lobe (Fig. 7D), and pSmad3 is readily detectable in the ventro-nasal retina and ventral POM, suggesting that TGF- β signaling is active in POM cells as they enter the choroid fissure (Fig. 7E, F'). At 32 hpf, neural crest cells are still present in the choroid fissure in numbers comparable to that of 28 hpf (Fig. 7G). A fraction of these cells have migrated dorsally behind the lens, where they form pericytes that line the hyaloid vasculature that forms here (Fig. 7G) (Trost et al. 2013). At this stage, ventro-nasal retinal pSmad3 has faded; the only detectable pSmad3 in the eye corresponds to the proximal lens tissue (Fig. 7H). There is no longer a clear domain of neural crest cells that colocalize with the pSmad3 signal (Fig. 7I, I'). Taken together, these data suggest that neural crest cells may be regulated by TGF- β ligands in the ventro-nasal retina at 28hpf.

Bmp3 regulates neural crest cell numbers in the choroid fissure

Given that Smad3 phosphorylation is active in neural crest cells and that Bmp3 appears to regulate fissure closure via Smad3 phosphorylation, we hypothesized that Bmp3 is a regulator of periocular neural crest function. To test this, we crossed our *bmp3*^{-/-} mutant line to our *Tg(sox10:EGFP)* transgenic line of zebrafish, which fluorescently label neural crest cells. In wildtype embryos, we observe many neural crest cells lining the fissure, particularly around the nasal lobe at 28 hpf (Fig. 8A) ($n=18$ eyes). In contrast, there are visibly fewer neural crest cells in the ventral eye of *bmp3*^{-/-} mutant embryos (Fig. 8B) ($n=18$ eyes). When quantified, the average number of neural crest cells in the choroid fissure is significantly reduced in *bmp3*^{-/-} mutants (6.56 ± 1.04 cells) when compared to wildtype animals (10.0 ± 1.00 cells) (Student's *t* test, $t_{34}=4.76$, $p<0.0001$, Fig. 8C). To test whether Bmp3 regulates neural crest cell numbers in the fissure via Smad3 phosphorylation, wildtype and *bmp3*^{-/-} mutant embryos on a *sox10:GFP* transgenic background were treated with a suboptimal dose of SIS3 (Fig. 8E, G) or an equivalent volume of DMSO (Fig. 8D, F) and the number of cell in the choroid fissures was quantified (Fig. 8H). As expected, there were significantly fewer neural crest cells in the fissures of eyes from *bmp3*^{-/-} mutants (8.33 ± 0.955 cells, $n=6$ eyes) compared to wildtype (10.8 ± 0.409 cells, $n=32$ eyes) when both groups were treated with DMSO (Student's *t* test, $t_{36}=2.43$, $p=0.0200$), which recapitulates the observations from Fig. 8A–C. When treated with SIS3, the number of neural crest cells is reduced in both wildtype and mutant fissures, suggesting that Smad3 phosphorylation is broadly required for the presence of neural crest cells in the fissure. Furthermore, we observe significantly fewer neural crest cells in the fissures of *bmp3*^{-/-} mutants treated with a suboptimal dose of SIS3 (7.19 ± 0.467 cells, $n=16$ eyes) compared to wildtype embryos treated with the same amount of inhibitor (8.81 ± 0.499 cells, $n=26$ eyes) (Student's *t* test, $t_{40}=2.20$, $p=0.0335$), indicating that mutations in *bmp3* sensitize neural crest cells in the choroid fissure to a suboptimal dose of SIS3, suggesting that *bmp3* regulates neural crest biology in the choroid fissure via Smad3 phosphorylation. Taken together, these data suggest that Bmp3 regulates the number of neural crest cells in the choroid fissure at 28 hpf, a timepoint that is critical for choroid fissure morphogenesis and closure.

Discussion

Despite being a significant cause of pediatric blindness, the genetic origins of coloboma are still incompletely understood. Here, we identify and characterize the role of *BMP3* in ocular morphogenesis and coloboma for the first time.

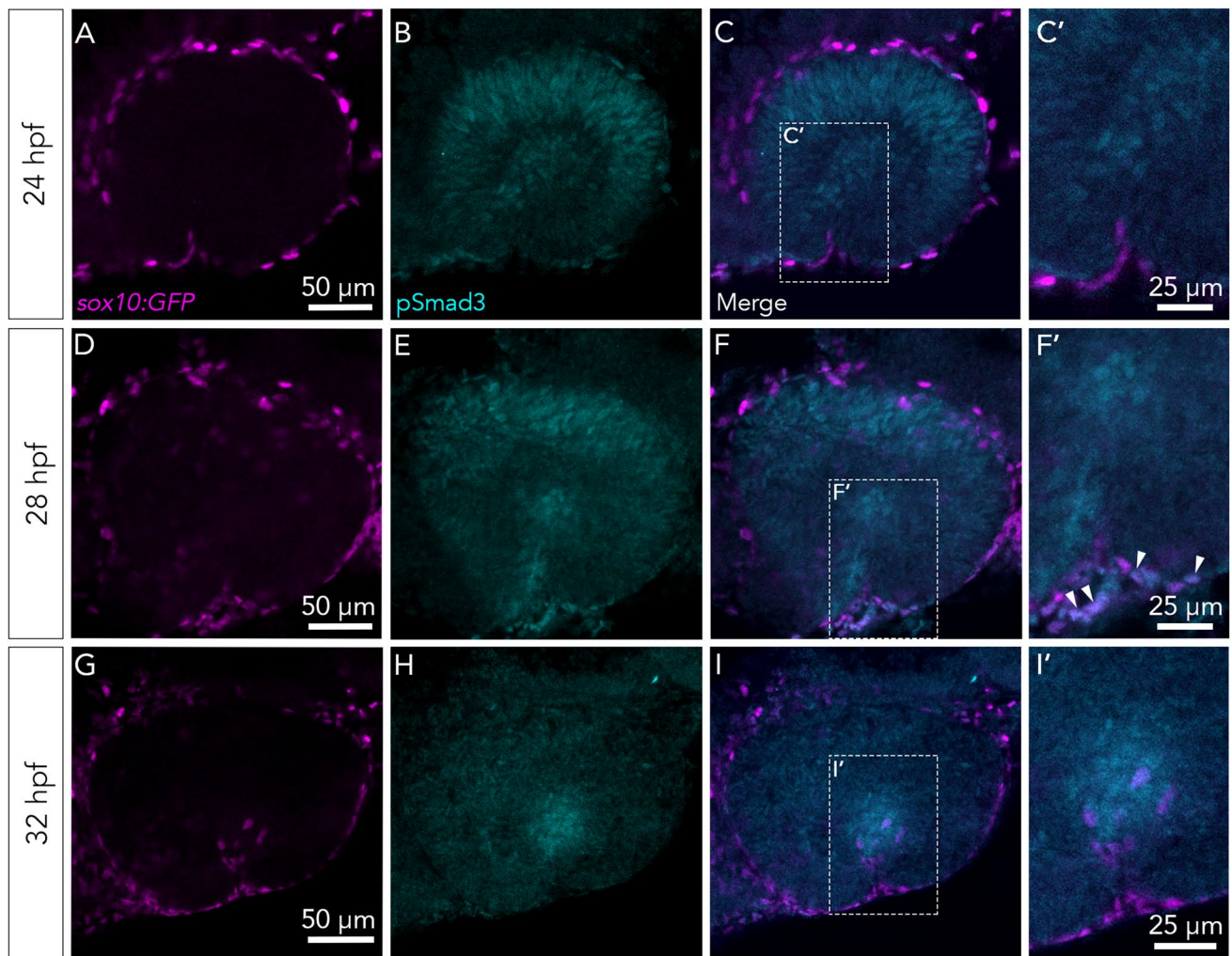


Fig. 7 Smad3 is phosphorylated in a subpopulation of periocular neural crest cells. pSmad3 immunofluorescence was conducted on wildtype *Tg(sox10:EGFP)* transgenic embryos at 24, 28, and 32 hpf. **A, C'** No colocalization of neural crest cells with pSmad3 is seen at 24 hpf. **D–F'** At 28 hpf there are several neural crest cells in the ven-

tral eye that colocalize strongly with pSmad3 (arrowheads). **G–I'** By 32 hpf, the colocalization between pSmad3 and *sox10*+neural crest cells in the ventral eye has diminished. The boxes in **C, F, and I** indicate the areas magnified in **C', F', and I'**, respectively. Images were taken of the proximal optic cup immediately posterior to the lens

Using both human patient data and zebrafish experimental evidence, we show that *BMP3* regulates choroid fissure closure through non-canonical Smad3 phosphorylation. We also provide evidence for *BMP3* regulating choroid fissure closure via the periocular mesenchyme, a process that remains poorly understood.

Studies performed using human patient data and model organisms have identified a number of loci that are involved in coloboma, collectively referred to as “the coloboma gene network” (Williamson and FitzPatrick 2014). Notably, genes that are overrepresented in this network encode components and downstream targets of developmental signaling pathways. This includes the TGF- β /BMP, sonic hedgehog, retinoic acid, fibroblast growth factor, and Wnt pathways (ALSomiry et al. 2019; Patel and Sowden

2019). This overrepresentation highlights the importance of developmental signaling pathways in ocular development, choroid fissure closure, and organ morphogenesis in general. This, in part, led us to choose *BMP3* as a candidate for investigation; BMPs have well characterized roles in the patterning of multiple organs, including the eye (Peters and Cepko 2002). Although some other candidates identified by WES are expressed in the developing eye, we were able to systematically eliminate them as candidates, as mutations in these genes are not significant contributors to MAC. Moreover, *BMP3* remained the most likely candidate due to its previously established role as a developmental signaling molecule (Bahamonde and Lyons 2001; Daluiski et al. 2001). Although *BMP3* was the most likely candidate for causing ocular disease in the pedigree

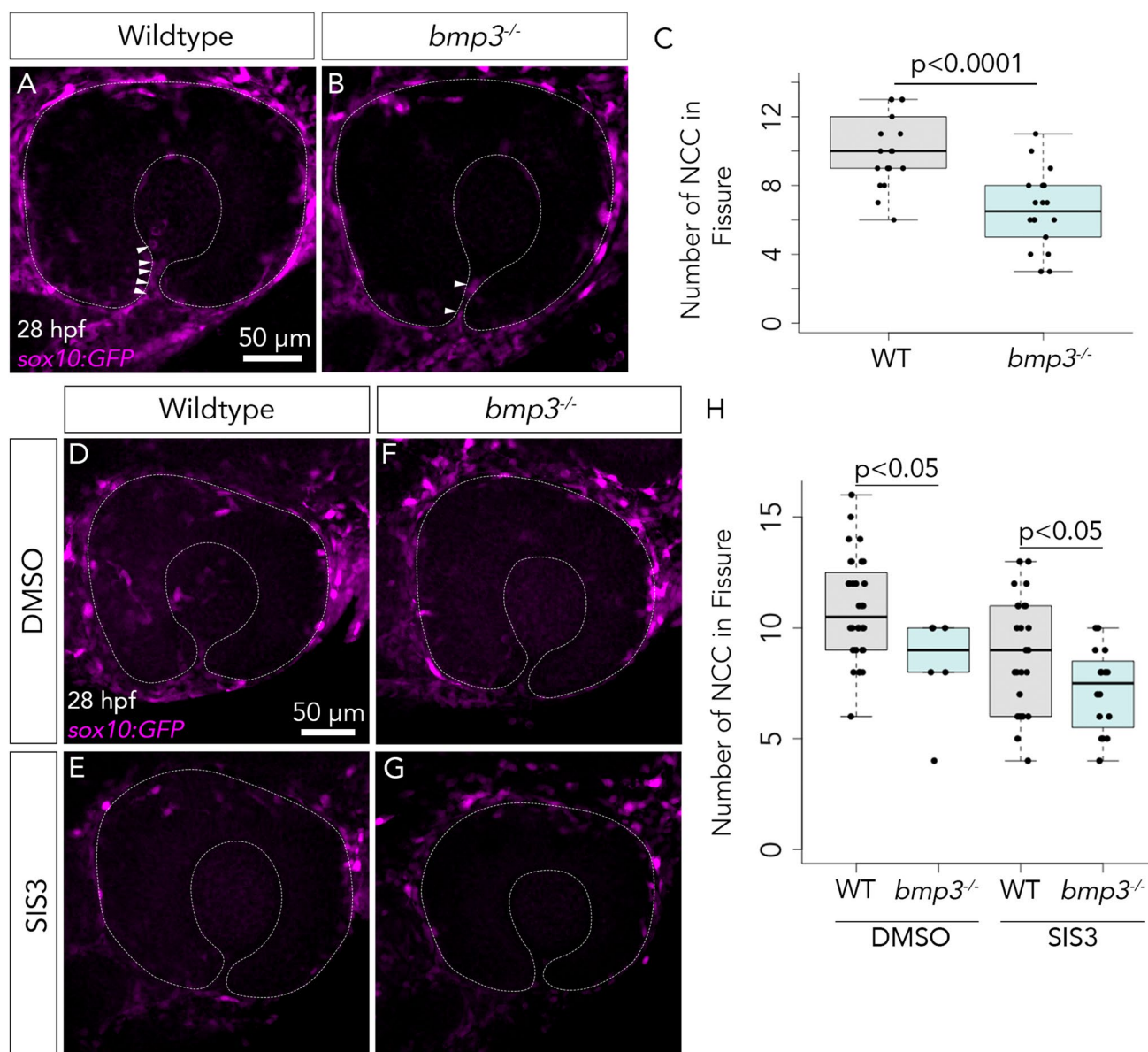


Fig. 8 Bmp3 regulates periocular neural crest cells. **A, B** To assess the effect of *bmp3* on periocular neural crest cells, the number of *sox10*+ cells was examined in *bmp3*^{-/-} mutants (**B**) and wildtype siblings (**A**) on a *Tg(sox10:EGFP)* transgenic background at 28 hpf. Images are maximum intensity projections of the stacks used to quantify cells in **C**. **C** There are significantly fewer neural crest cells in the choroid fissures of *bmp3*^{-/-} embryos (6.56 ± 1.04 cells, $n=18$ eyes) compared to wildtype siblings (10.1 ± 1.00 cells, $n=18$ eyes) (two sample *t* test, $t_{34}=4.76$, $p<0.0001$). **D–G** To determine whether Bmp3 regulates neural crest cells via Smad3 phosphorylation, wildtype (**E**, $n=26$) and *bmp3*^{-/-} mutant (**G**, $n=16$) were treated with a suboptimal dose of Smad3 inhibitor. Wildtype (**D**, $n=32$) and

bmp3^{-/-} mutants (**F**, $n=6$) were also treated with DMSO as controls. Images are maximum intensity projections of the stacks used to quantify cells in **H**. **H** Quantification of **D–G**. When treated with DMSO, eyes from *bmp3* mutant embryos show significantly fewer neural crest cells in the fissure (8.33 ± 0.954 cells) than wildtype counterparts (10.8 ± 0.409 cells) (Student's *t* test, $t_{36}=2.43$, $p=0.0200$). When treated with SIS3, eyes from *bmp3*^{-/-} mutant embryos have significantly fewer neural crest cells in localized to the fissure (7.19 ± 0.467 cells) compared to eyes from wildtype embryos (8.81 ± 0.499 cells) (Student's *t* test, $t=2.20$, $p=0.033$), suggesting that Bmp3 regulates the presence of neural crest cells in the fissure via Smad3 phosphorylation. Dotted lines indicate the outline of the optic cup. WT wildtype

analyzed, there were other loci, including *SEMA5B* and *CRYAA*, which were attractive candidates for study due to their previously documented roles in eye development and function (Matsuoka et al. 2011; Sun et al. 2017). Although we were able to systematically rule these loci out as being

the most likely cause of coloboma in the pedigree, we cannot rule out the possibility that mutations in these loci are contributing to disease as modifier loci. With the advent of genome editing techniques such as CRISPR/Cas9, studying the role of multiple loci and complex patterns

of inheritance in the etiology of coloboma is becoming more feasible.

In addition to the *BMP3* variant identified by our WES experiments (A470P), the two additional *BMP3* variants (S393F and F450Y) identified from Sanger sequencing 154 unrelated MAC patients strongly suggests that *BMP3* is a locus involved in the etiology of coloboma. These variants are extremely rare, suggesting that they are not benign variants found in the general population; rather, it is likely that these variants contribute to the etiology of MAC in these patients. This is supported by both predictive algorithms of protein folding and cell secretion assays, which show that at least two of the variants, A470P and S393F, result in the absence of these variant proteins from the media of COS-7 cells. Both A470 and S393 are located near cysteine residues that participate in the disulfide bonds that are critical for the stability of mature BMP3 dimers. Therefore, the presence of amino acid substitutions at either of these residues may result in aberrant cysteine knot formation, resulting in lowered extracellular stability of BMP3 and thus its absence from the cell culture media (Goebel et al. 2019). Interestingly, there is another variant at the A470 residue listed in gnomAD (p.Ala470Thr) that is present in control individuals (7/75 435 individuals). Although this may suggest that change to the A470 residue do not cause changes to BMP3 activity, the A470T amino acid change is, relative to A470P, conservative; threonine is small and uncharged, making it unlikely that it dramatically affects BMP3 protein structure and function. Proline, on the other hand, forms a pyrrolidine loop with the nitrogen from the amino acid backbone. This pyrrolidine loop has previously been observed to dramatically disrupt the secondary structure of proteins, therefore, making it exceptionally likely that this amino acid disrupts BMP3 protein structure (Levitt 1978). Although S393F and A470P are likely pathogenic, the molecular mechanism of their pathogenicity remains unclear. Neither of the variant proteins are secreted at full levels, however, whether the phenotypes seen in patients are due to haploinsufficiency or a dominant negative effect is currently unknown. On one hand, misfolding of the variant proteins could cause their retention and degradation in the cell, leading to less secreted protein overall, suggesting haploinsufficiency. On the other hand, misfolding of the variant protein could lead to aggregation of both the wildtype and variant BMP3 protein, leading to a dominant negative mechanism. Taken together, this evidence strongly suggests that the patient variants identified through WES and Sanger sequencing have deleterious consequences to protein activity, further implicating *BMP3* as a novel coloboma-causing locus.

For the third variant detected, F450Y, we do not observe any secretion aberrancies. This residue is located in close proximity to the receptor-binding domain of the BMP3 protein (Allendorph et al. 2007). The receptor binding domain

of BMP3 is extremely sensitive to amino acid composition, and single amino acid substitutions have been shown to reduce its affinity for its receptor (Allendorph et al. 2007). Alternatively, this residue may not be pathogenic; this is supported by the presence of this variant in control genome databases (Table 2). Therefore, more investigation is needed to confirm whether BMP3-F450Y is a pathogenic variant.

We show that zebrafish *bmp3*^{-/-} mutants have an incompletely penetrant coloboma phenotype. Additionally, we show that this phenotype is a delay in fissure closure, as all *bmp3*^{-/-} mutants assayed have closed fissures at 72 hpf. The nature of the choroid fissure closure defects observed in these mutants may give some indication as to *bmp3*'s role in fissure closure. It has been proposed that coloboma can be broadly separated into two classes: morphogenetic coloboma, which arises from defects the morphogenesis of the eye cup, and fusion defective coloboma, which arises from defects in degradation of the basal lamina or adhesion of the retinal cells that make up the choroid fissure (James et al. 2016; Eckert et al. 2020). Eyes from *bmp3*^{-/-} mutants are not smaller in size than those from wildtype embryos, and the fissure lobes are fully apposed without any gross morphological defects, suggesting that *bmp3* is not a regulator of early ocular morphogenetic events such as optic vesicle evagination or choroid fissure formation, as perturbations to these process usually cause overt morphological defects such as microphthalmia and severe, very obvious coloboma (Patel and Sowden 2019). Due to the subtlety of the choroid fissure closure defects in *bmp3* mutants, it is more likely that *bmp3* facilitates processes that occur later in choroid fissure closure, such as basement membrane breakdown or intercalation of the retinal cells that make up the lobes of the choroid fissure. Indeed, the phenotypes of *bmp3* mutants resemble other zebrafish models of defective basement membrane degradation and cellular intercalation, further suggesting that *bmp3* plays a role in these processes (James et al. 2016; Hardy et al. 2019).

Previous studies of *bmp3* function have shown that it non-canonically activates the phosphorylation of Smad2/3 rather than Smad1/5/8 (Bahamonde and Lyons 2001; Daluiski et al. 2001; Stewart et al. 2010). We show that *bmp3* is likely facilitating choroid fissure closure through this mechanism, as indicated by the presence of phospho-Smad3 adjacent to the fissure and the increased sensitivity of *bmp3*^{-/-} embryos to SIS3. Recent work on zebrafish has shown that there are other TGF- β ligands expressed in the fissure, and that TGF- β signaling is active in the fissure at the same time we detect phospho-Smad3 in the retina (Knickmeyer et al. 2020). Therefore, *bmp3* may act in concert with other TGF- β ligands to facilitate choroid fissure closure (Knickmeyer et al. 2020). The mechanism behind this process is still not clear; others have proposed that TGF- β signaling via Smad2/3 phosphorylation in the fissure promotes the

expression of BMP antagonists which leads to the inhibition of dorsal BMP signaling (Knickmeyer et al. 2020). This thereby creates a restricted domain of BMP expression in the dorsal eye and conferring dorsal identity (Knickmeyer et al. 2020). Indeed, BMP3 has been shown to inhibit both canonical BMP signaling and Activin signaling (Gamer et al. 2005; Knickmeyer et al. 2020). This mechanism has also been well documented in other developmental processes including axis patterning and gastrulation (Little and Mullins 2006). However, this is somewhat at odds with our results; we do not observe any changes to the expression of dorsal markers, especially *tbx5a*, which is a direct transcriptional output of BMP signaling in the dorsal eye, suggesting that *bmp3* does not antagonize dorsal BMP signaling. Therefore, more research is needed to determine the precise pathway through which Bmp3 inhibits canonical BMP signaling in eye development.

Interestingly, *bmp3* is not expressed in the dorsal eye like other ocular BMP ligands, such as *gdf6a* (French et al. 2009; Gosse and Baier 2009). Rather, it is expressed in the ventral head mesenchyme adjacent to the fissure. The head mesenchyme is populated by both cranial neural crest cells and paraxial and splanchnic mesoderm (Creuzet et al. 2003; Gage et al. 2005). Accordingly, there has been evidence that *bmp3* functions in both the mesoderm and the cranial neural crest; *bmp3* expression has been detected in the tail paraxial mesoderm of zebrafish and has also been shown to be a regulator of neural crest-derived craniofacial structures (Mueller et al. 2010; Schoenebeck et al. 2012). Here, we provide evidence that *bmp3* is a regulator of cranial neural crest cells rather than cranial mesoderm, as indicated by micro-CT scans of adult fish and Alcian blue staining of larval jaw cartilage. Although this is consistent with other reports of *bmp3* function, we find that the larval mutant phenotypes are far less severe and have lower penetrance than previously reported (Schoenebeck et al. 2012). However, these previous studies were performed using morpholino oligonucleotides, which have been shown to produce more severe phenotypes when compared to mutants (Eve et al. 2017). Regardless, we provide further evidence that *bmp3* regulates neural crest-derived structures and is novel regulator of craniofacial development, particularly structures that contribute to the jaw. This is somewhat unsurprising, as craniofacial abnormalities and coloboma commonly occur together in syndromes including CHARGE syndrome and BOFS syndrome (Siebert et al. 1985; Gestri et al. 2009). These studies, together with our own studies of *BMP3*'s involvement in coloboma, suggest that there is likely a shared neural crest-derived etiology of coloboma and craniofacial abnormalities in many contexts (Gestri et al. 2009; Bajpai et al. 2010). At the time of DNA collection, the human patients were not assessed for craniofacial abnormalities, and since these patient DNA samples are archival and were analyzed

more than 20 years after collection, it is not feasible to determine whether these patients had craniofacial abnormalities. However, it wouldn't be entirely surprising to find craniofacial abnormalities in patients with damaging mutations in *BMP3*, given that we see craniofacial abnormalities in our zebrafish model. Interestingly, the phenotypes observed in *bmp3* mutants in this study all have varying degrees of penetrance, with delayed fissure closure being the phenotype with the lowest penetrance (~18%), the midface hypoplasia being the highest (100% of observed mutants), and the chondrocyte morphology phenotype sitting in between the two phenotypes (~40%). Although the reason why these phenotypes appear with different penetrance is not clear, we hypothesize that it is due, at least in part, to the fact that *bmp3* likely functions alongside other TGF- β ligands during development, and the relative contribution of these accompanying ligands during development could differ between tissues (i.e. periocular region and jaw) and developmental timepoints (i.e. embryonic, larval, juvenile and adult stages).

In our studies of cartilage development in *bmp3*^{-/-} mutants, we observe jaw chondrocytes that are less organized and undifferentiated when compared to wildtype controls, suggesting that *bmp3* doesn't affect the migration of neural crest cells to form the cartilage, but rather regulates the differentiation of cranial neural crest cells into chondrocytes. Moreover, only anterior structures derived from pharyngeal arch 1 and 2 (such as Meckel's cartilage, the palatoquadrate, and the ceratohyal) are affected, whereas structures derived from the more posterior pharyngeal arches 3–7 (such as the ceratobranchials) remain largely unaffected, suggesting that *bmp3*'s role on craniofacial development is restricted to the neural crest cells of the first pharyngeal arch; indeed, other studies of *bmp3*'s role on craniofacial development found its expression to be highest in the anterior pharyngeal arches and lower or absent in the more posterior arches (Schoenebeck et al. 2012). This suggests that *bmp3* may be regulating the differentiation of arch 1 and 2 neural crest cells, and the absence of *bmp3* in the first arch results in undifferentiated chondrocytes and, thus, the craniofacial defects we observe in *bmp3*^{-/-} mutants. Alternatively, *bmp3* could be regulating cranial neural crest cell division, survival, or death; a lack of *bmp3* results in an incorrect number of chondrocyte precursors, which, ultimately, results in disorganization of the cartilage seen in *bmp3* mutants. Consistent with this, there appears to be more chondrocytes present in the jaws of *bmp3*^{-/-} mutants. Once the cranial neural crest cells condense into cartilage, convergence extension elongates the chondrocytes and facilitates chondrocyte stacking (Kimmel et al. 1998). Other studies have shown that disrupting genes necessary for convergence extension results in jaw phenotypes similar to *bmp3*^{-/-} mutants, suggesting that *bmp3* could have a role in regulating the number of cells necessary for convergence extension to occur properly

(Rochard et al. 2016). Further research is needed to establish the precise role of *bmp3* in craniofacial development and cranial neural crest function.

In addition to regulating the neural crest-derived craniofacial skeleton, we also show that *bmp3* regulates periocular neural crest cells during choroid fissure closure. There have been several studies that have shown that these populations of cells are necessary for choroid fissure closure, further solidifying the role of these cells as necessary mediators of choroid fissure closure (James et al. 2016; Gestri et al. 2018). This is also supported by our studies, where ventral periocular neural crest cells colocalize with pSmad3 signal, suggesting that neural crest cells are responsive to TGF- β signaling. This is in agreement with other studies of periocular neural crest cells and TGF- β signals, which show that neural crest-specific deletion of *Tgfb2* results in compound ocular defects in mice (Ittner et al. 2005). Therefore, this represents a plausible mechanism for TGF- β signaling in the eye, where cranial neural crest cells are responsive to Bmp3 and potentially other TGF- β ligands. This also fits with our model of Bmp3 facilitating later stages of choroid fissure closure; although some reports of neural crest-mediated choroid fissure closure have shown that periocular neural crest cells are necessary for early eye vesicle morphogenesis, others have proposed that neural crest cells are necessary for later stages of choroid fissure (James et al. 2016; Gestri et al. 2018; Hardy et al. 2019; Bryan et al. 2020). We also observe a reduction in the number of neural crest cells in the choroid fissures of *bmp3*^{-/-} mutants at 28 hpf, suggesting that Bmp3 regulates the number of neural crest cells in the choroid fissure. However, it is unclear whether Bmp3 regulates neural crest number, guidance, or differentiation. Previous reports and our own studies of Bmp3 function in craniofacial development have shown that the neural crest-derived craniofacial cartilage is severely reduced in *bmp3* morphants, suggesting that *bmp3* plays a role in neural crest differentiation (Schoenebeck et al. 2012). In contrast, other reports of periocular neural crest migration suggest that TGF- β signals emanating from the lens regulate periocular neural crest migration into the anterior segment (Takamiya et al. 2020). Therefore, it is plausible that ocular TGF- β signals are also necessary for facilitating migration of periocular neural crest cells into the choroid fissure.

In summary, we present the discovery of a novel locus involved with choroid fissure closure, *BMP3*. We have shown that BMP3 likely facilitates fissure closure through Smad3 phosphorylation, and we also provide evidence that BMP3 may regulate periocular neural crest cells during the process of fissure closure. Although the present study has advanced our understanding of choroid fissure closure biology and, thus, coloboma, further work will need to be done to identify additional loci that are involved in this process. Additionally, more investigation is warranted to identify and

characterize loci that are expressed by the periocular mesenchyme and their role in choroid fissure closure as well as paracrine factors that regulate the periocular mesenchyme which will, in turn, inform our understanding of vertebrate ocular morphogenesis.

Materials and methods

Whole exome and Sanger sequencing of human patient DNA

Whole exome sequencing (WES) was performed on genomic DNA from each proband as part of FORGE Canada Consortium at the McGill University and Genome Quebec Innovation Centre. Exome target enrichment was performed using the Agilent SureSelect 50 Mb (V3) All Exon Kit and sequencing was performed on the Illumina HiSeq 2000, multiplexing three samples per lane. The mean coverage of coding sequence regions, after accounting for duplicate reads was greater than 70x. WES data were analyzed by performing alignment with BWA, duplicate read removal with Picard, local indel realignment with GATK, variant calling with SAMtools, and annotation with Annovar and custom scripts.

For Sanger sequencing of the MAC patient cohort unrelated to individuals in the pedigree from Fig. 1, intronic primers were used to amplify *BMP3* in 154 patients with MAC. The amplicons were then purified and sent for Sanger sequencing at the Genome Quebec Innovation Centre.

Zebrafish husbandry

Adult zebrafish were kept on a 10-h dark/14-h light schedule. Embryos were raised at 25.5 °C, 28.5 °C or 33 °C in embryo media and staged according to standardized developmental hallmarks (Kimmel et al. 1995). Embryos that were grown past 24 hpf were treated with 0.004% 1-phenyl 2-thiourea (PTU, Sigma Aldrich P7629) prior to 22 hpf to block pigment formation. Anesthesia of larval and adult zebrafish was performed with a 4% dilution of 0.4% tricaine methanesulfonate (TMS) stock solution (Sigma Aldrich E10521). The AB wildtype strain, the *bmp3*^{-/-} mutant line, and the *Tg(sox10:EGFP)* transgenic line were used. The *bmp3*^{-/-} line contains two in-frame 3 basepair (bp) deletions (NM_001077765.1:c.543_545del and NM_001077765.1:c.840_842del) and a 5 bp deletion (NM_001077765.1:c.886_890del). Both of the 3 bp deletions cause the deletion of a single glutamine residue (NP_001071233.1:p.Gln182del and NP_001071233.1:p.Gln281del). The 5 bp deletion results in a frameshift and premature stop codon upstream of the mature TGF- β signaling domain (NP_001071233.1:p.Thr296GlyfsTer2).

Atomic Non-Local Environment Assessment (ANOLEA)

Using the previously solved crystal structure for BMP3, the effect of patient amino acid substitutions on protein function were modeled in silico using Swiss-pdb Veiwier and analyzed using the ANOLEA server (<http://melolab.org/anolea/>) (Melo et al. 1997; Allendorph et al. 2007). Using the ANOLEA data, the difference in energy requirement needed to fold the BMP3 protein with each amino acid substitution was plotted in Microsoft Excel.

Site-directed mutagenesis

The open reading frame for wildtype human *BMP3* was obtained from ASU BioDesign Institute in pDNR-Dual and was moved into pcDNA3.2/V5. Oligonucleotide primers for site-directed mutagenesis were designed to generate constructs carrying c.1178C > T (p.S393F), c.1349 T > A (p.F450Y), and c.1408G > C (p.A470P) variants individually. The PCR reaction for site-directed mutagenesis contained: 500 ng of template plasmid DNA, 17 µl of master mix (100 µl 10× PFU buffer, 792 µl water, 2 µl each of 100 mM dNTPs), 1 µl (10 mM) NAD, 0.5 µl (200 ng) each primer, 0.5 µl DMSO, 0.3 µl Taq DNA Ligase (NEB, M0208S), 1 µl PfuUltra DNA Polymerase (Agilent, 600670), and 1.5 µl water. The PCR cycle conditions were denaturation at 95 °C for 2 min, then 30 cycles of 95 °C for 1 min, 55 °C for 1 min, and 65 °C for 10 min. PCR products were then digested with 1 µl of DpnI (NEB, R0176S) for 30 min at 37 °C to digest the original plasmid. Constructs were verified by Sanger sequencing to ensure the mutation was introduced correctly. DNA for the four constructs was isolated by maxi prep (Qiagen, 12165) and Sanger sequenced to confirm the mutation sites.

Tissue culture and immunoblotting

COS-7 cells were plated to 6-well dishes and transfected at 80% confluency. 3 µg of DNA was transfected per well using Lipofectamine 2000 (ThermoFisher Scientific, 12566014) according to the manufacturer's instructions. Transfected cells were grown in low serum (0.1%) conditions for 48 h and then harvested. Media was removed and saved for secreted protein analysis. Cell monolayers were rinsed once in phosphate buffered saline (PBS), and 500 µl of cold lysis buffer was added. Lysis buffer components were 50 mM Tris, 150 mM NaCl, 1 mM EDTA, 1.5% SDS, and one complete mini protease inhibitor tablet (Millipore/Sigma 11836170001), pH 7.5. Cells sat on ice for 10 min and were then scraped and collected in Eppendorf tubes. Samples were boiled, transferred to QiaShredder tubes (Qiagen, 79656), centrifuged, and the flow-through was collected in

new tubes. Proteins from media were concentrated by acetone precipitation (1:1.5 media to acetone volume) and air dried. A minimal volume of lysis buffer was added to resuspend the pellets. Protein concentration was determined using the Bradford colorimetric protein assay (BioRad, 5000201). Cell lysates and concentrated media lysates were run on 4–12% Bis-Tris gradient gels (Invitrogen NP0336) for 1 h at 200 V. Resolved proteins were transferred to polyvinylidene difluoride (PVDF) membranes (Millipore IPVH00010) at 22 V for 1 h on a semi-dry blotter (Amersham Biosciences). Blots were blocked in 5% milk in Triton buffered saline with Tween 20 (TBST) for 2 h and primary antibody was added for overnight incubation at 4 °C. Mouse monoclonal anti-V5 primary antibody (ThermoFisher, MA5-15253) was used at 1:5000 dilution in 5% milk and mouse monoclonal anti-tubulin primary antibody (Sigma, T9026) was used at 1:10,000. After washing, sheep anti-mouse IgG HRP-conjugated secondary (Amersham, NA931) was added at 1:5000 for 1 h at room temperature. Membranes were washed in SuperSignal West Pico PLUS ECL reagent (ThermoFisher, 34577) for 3 min and detection was performed using the ChemiDoc MP Imaging System (BioRad).

CRISPR/Cas9 mutagenesis

Short guide RNA (sgRNA) design and synthesis were performed as previously described (Gagnon et al. 2014). The sequences for the oligonucleotides used to generate the templates for sgRNA synthesis are: 5'-GGGACTTCATCTCAT GGCAGTGG-3', 5'-GGGAGCTCATTGTTCTGCAGTGG-3' and 5'-GGCTGGCCTCATCCCATGTAGGG-3'. Cas9 protein (PNA Bio, CP01) was reconstituted in sterile water to a concentration of 50 µg/mL and 2 µL was mixed with 1 µL of each sgRNA. One- or two-cell stage embryos were injected with 1 nL of Cas9/sgRNA mixture and allowed to develop to sexual maturity. Carriers for frameshift mutations were identified by high resolution melt (HRM) analysis using the Type-It HRM PCR kit (Qiagen, 206544) on a Rotor Gene Q qPCR machine (Qiagen, 9001560) and Sanger sequencing.

Zebrafish genotyping

bmp3^{-/-} mutants were genotyped using polymerase chain reaction (PCR) followed by gel electrophoresis. Genomic DNA was extracted from fin clips in 20 µL of 50 mM NaOH at 95 °C for 15 min and subsequently neutralized using 2 µL Tris-HCl, pH 8.0. Samples were diluted 1/2 in sterile water and used as template for PCR using the following primers: Forward: 5'-CTTCATATGCTGGAATCGCATAAC-3', Reverse: 5'-TTGCTCTCCATCGGATCATAAG-3'. PCR was performed using the following conditions: Denaturation at 94 °C for 2 min, 40 cycles of 94 °C for 15 s, 58 °C for

15 s, and 72 °C for 12 s, followed by a final extension cycle at 72 °C for 3 min. PCR products were then run on a 3% agarose gel to resolve the wildtype and mutant amplicons (167 bp and 156 bp, respectively).

Quantitative real-time PCR (qRT-PCR)

Total RNA was extracted from at least 40 embryos at 22 hpf using RNAqueous-4PCR (Ambion) and purified using the RNeasy Mini Kit (Qiagen). First-strand synthesis was performed using the AffinityScript qPCR cDNA Synthesis Kit (Agilent) using random primers according to the manufacturer's specifications. qPCR analysis was performed using Brilliant II SYBR Green qPCR Master Mix (Agilent) as previously described (Pillay et al. 2010). qRT-PCR reactions were run on a Rotor Gene Q qPCR machine (Qiagen, 9001560). Primers were validated prior to the experiment, as previously described (Pillay et al. 2010). Endogenous control primers (elongation factor 1a; *ef1a*), previously used (Pillay et al. 2010), were chosen from the Universal Probe Library Assay Design Centre for Zebrafish (Roche). The sequences for qPCR primers used are: *bmp3* Forward: 5'-GCAGATGCTCTACGCCAAATA-3', *bmp3* Reverse: 5'-GGTGAGGGAAGTGAGGTTAAAG-3', *ef1a* Forward: 5'-CCTTCGTCCCAATTTTCAGG-3', *ef1a* Reverse: 5'-CCTTGAACAGCCCATGT-3'. qRT-PCR data were analyzed as previously described (Livak and Schmittgen 2001).

In-situ hybridization

Antisense riboprobes labeled with digoxigenin (DIG) were synthesized from purified, linearized expression plasmid containing a gene-specific insert or from a gene-specific PCR product with an integrated T7 RNA polymerase site. Probe synthesis was performed as previously described (Thisse and Thisse 2008).

Embryos were fixed overnight at 4 °C in 4% paraformaldehyde (PFA) and subsequently permeabilized for 5 min at room temperature (RT) using 10 µg/ml Proteinase K in PBST. Single-color and two-color in-situ hybridization was performed as previously described except probes were not hydrolyzed (Prince et al. 1998). For experiments analyzing *bmp3* or *bmp3/crestin* expression, embryos were either manually de-yolked and flat-mounted under a coverslip in 70% glycerol or embedded in paraffin wax, sectioned, and mounted under a coverslip using Dibutylphthalate Polystyrene Xylene (DPX) mountant. Flat-mounts and sections were imaged on a Zeiss AxioImager Z1 compound microscope with AxioCam HR digital camera. For experiments analyzing *tbx5a*, *alhd1a2*, *vax2* and *alhd1a3* expression, embryos were mounted in 3% methyl-cellulose on a spot plate and imaged

with an Olympus SZX12 stereomicroscope and Qimaging micropublisher camera.

Immunofluorescence

For laminin immunofluorescence, embryos were fixed in 4% PFA for 2 h at RT. Embryos were permeabilized with 10 µg/ml Proteinase K for 30 min. After permeabilization, embryos were blocked for at least 1 h at RT using 5% normal goat serum and 2% bovine serum albumin (BSA) in PBST. Embryos were incubated O/N in rabbit anti-laminin primary antibody diluted in block (1:200, L-9393, Sigma-Aldrich). After washing, embryos were incubated for 2 h at RT in goat anti-rabbit Alexa Fluor 555 secondary antibody (1:1000, A32732, Invitrogen).

For Phosphorylated Histone H3 immunofluorescence, embryos were fixed in 4% PFA for 2 h at RT. Embryos were permeabilized in ice-cold acetone for 7 min at −20 °C. After permeabilization, embryos were incubated in 10 mM citric acid at 95°C for 10 min for antigen retrieval. Embryos were then blocked in 3% BSA in 0.5% TritonX-100 in PBS for 1 h at RT. Embryos were then incubated in rabbit anti-phospho-Histone H3 antibody (1:1000, ab183626, Abcam) O/N at 4 °C, washed, and incubated in goat anti-rabbit Alexa Fluor 488 secondary antibody (1:1000, A32732, Invitrogen) plus TO-PRO-3 (1:1000, T3605, Invitrogen) for 2 h at RT.

For cleaved Caspase 3 immunofluorescence, embryos were fixed in 4% PFA for 2 h at RT. Embryos were permeabilized with ice-cold acetone for 7 min at −20 °C. After permeabilization, embryos were blocked in 5% goat serum (GS) in PBS/DTT (PBST + 1% DMSO + 0.1% TritonX-100) for 2 h at RT. Embryos were then incubated in rabbit anti-cleaved-Caspase3 (1:400, 559565, BD Biosciences) O/N at 4 °C, washed, and incubated in goat anti-rabbit Alexa Fluor 488 secondary antibody (1:1000, A32732, Invitrogen) plus TO-PRO-3 (1:1000, T3605, Invitrogen) for 2 h at RT.

For phosphorylated Smad3 (pSmad3) immunofluorescence, embryos were fixed overnight at 4 °C. Embryos were permeabilized with 10 µg/ml Proteinase K for 5 min. After permeabilization, embryos were incubated in 4% BSA in 0.15% TritonX-100 in PBS. Embryos were incubated in rabbit anti-pSmad3 primary antibody (1:200, ab59203, Abcam) O/N at 4 °C, washed, and incubated in goat anti-rabbit Alexa Fluor 488 or 568 secondary antibody O/N at 4 °C (1:1000, A32732, Invitrogen).

After immunofluorescence was performed, embryos were washed and passed through a 30, 50, and 70% glycerol series. Eyes and the surrounding head mesenchyme were dissected from whole embryos and mounted in 70% glycerol on a glass slide. All immunofluorescence

experiments were imaged using a Zeiss AxioImager Z1, Zeiss LSM700 laser scanning confocal microscope.

Pharmacological inhibition of TGF- β signaling

To inhibit TGF- β signaling, Specific Inhibitor of Smad3 (SIS3) was used (566405-1MG, Calbiochem). The structure and activity of SIS3 has been described elsewhere (Jin-nin et al. 2006). 1 mg of SIS3 was resuspended in DMSO to a stock concentration of 3 mM, aliquoted, and stored at -20°C . Prior to treatment, the stock was mixed with pre-warmed embryo media to a final concentration of 12 μM . For controls, an equivalent volume of DMSO alone was added to pre-warmed embryo media. Embryos were stage-matched at 10 hpf. At 24 hpf, embryos were dechorionated, transferred to 35 mm petri dishes in groups of 15 embryos per dish, and 5 mL of SIS3- or DMSO-treated media was added to the appropriate dishes. Embryos were incubated for at 28.5 $^{\circ}\text{C}$ for 4 h until 28 hpf (Fig. 8) or for 6 h until 30 hpf (Fig. 5). The media was then removed and embryos were washed 3 times with fresh embryo media. Embryos were then either fixed in 4% PFA (Fig. 8) or all dishes were returned to 28.5 $^{\circ}\text{C}$ (Fig. 5). Embryo media was changed at 48 hpf, and embryos were fixed at 72 hpf for 2 h at RT with 4% PFA. Embryos were then used for laminin immunofluorescence. Eyes from these embryos were then dissected, mounted on glass slides in 70% glycerol, and imaged using a Zeiss AxioImager Z1, Zeiss LSM700 laser scanning confocal microscope.

Micro-computed tomography (micro-CT) of adult zebrafish

18-month-old wildtype ($n=5$) and *bmp3*^{-/-} ($n=5$) zebrafish were scanned using MILabs μCT at the School of Dentistry, University of Alberta. Zebrafish were fixed at 4% PFA for 24 h. The parameters for scanning and reconstruction were conducted as previously described (Miyashita et al. 2020). AVIZO (Life Technologies) software was used to visualize and quantify premaxilla, maxilla, and mandible length. Landmarks used to quantify the midfacial region are demonstrated in Fig. S7.

Alcian blue staining of larval zebrafish

Alcian blue staining of 7 dpf larval zebrafish was performed as previously described, except Alizarin red staining was not performed (Walker and Kimmel 2007). Briefly, larval zebrafish were euthanized using a 4% dilution of 0.4% TMS and fixed in 1% PFA for 1 h at RT. Embryos were washed for 10 min in 10 mM MgCl_2 buffered with 100 mM Tris pH 7.5, and then stained overnight in 0.04% Alcian blue staining solution. Embryos were removed from staining solution,

rehydrated, bleached for 10 min in 3% H_2O_2 /0.5% KOH, and de-stained with two 10-min washes of 25% Glycerol/0.1% KOH and two 10-min washes of 50% Glycerol/0.1% KOH. Embryos were then transferred to 70% glycerol and mounted on glass slides for imaging. Images were taken using a Zeiss AxioImager Z1 compound microscope with AxioCam HR digital camera.

Confocal imaging

All fluorescent images were taken on a Zeiss AxioImager Z1, Zeiss LSM700 laser scanning confocal microscope using a Zeiss Plan Apochromat 20/0.8 objective lens. Z-stacks were made by taking optical slices at intervals of 2–3 μm for a total of 8–12 slices per sample. Maximum intensity projections were created from the resulting stacks using ImageJ software.

Cell quantification

Cell quantification was performed by hand using the Multi Point tool in ImageJ to mark which cells had been counted. For quantification of pSmad3+ cells (Fig. 5), a single z-stack representative of the proximal retina was used. Only pSmad3+ cells in the lower-nasal quadrant were counted. For quantification of neural crest cells (Fig. 7), a series of z-stacks spanning the entire choroid fissure was used. Only cells that were present in the fissure were counted. The area of the choroid fissure was defined as the space between each choroid fissure lobe, the lens, and the margin of the eye cup.

Statistical analysis

Statistical significance was determined using Fisher's exact test (Fig. 2), a two-proportion z test (Fig. 5) or Student's t test (Figs. 5, 6, 7, and S4). Quantitative results are presented as percentage or mean \pm standard error.

Supplementary Information The online version contains supplementary material available at <https://doi.org/10.1007/s00439-022-02430-3>.

Acknowledgements The authors are grateful to Science Animal Support Services for zebrafish animal care and facility maintenance.

Funding This work was funded by the Women and Children's Health Research Institute (UOFAB WCHRIIG 2879) and the National Science and Engineering Research Council of Canada (NSERC RGPIN-2016-04682).

Availability of data and material The data that support the findings of this study are available from the corresponding author upon reasonable request.

Code availability Not applicable.

Declarations

Conflict of interest The authors declare no conflicts of interest.

Ethics approval Embryonic, larval, and adult zebrafish were cared for according to guidelines set by the Canadian Council of Animal Care and protocols were approved by the University of Alberta's Animal Care and Use Committee (Protocol #427).

Consent to participate Not applicable.

Consent to publish Not applicable.

References

- Abouzeid H, Boisset G, Favez T et al (2011) Mutations in the SPARC-related modular calcium-binding protein 1 gene, SMOC1, cause waardenburg anophthalmia syndrome. *Am J Hum Genet* 88:92–98
- Adler R, Belecky-Adams TL (2002) The role of bone morphogenetic proteins in the differentiation of the ventral optic cup. *Development* 129:3161–3171
- ALSomiry AS, Gregory-Evans CY, Gregory-Evans K (2019) An update on the genetics of ocular coloboma. *Hum Genet* 138:865–880. <https://doi.org/10.1007/s00439-019-02019-3>
- Allendorph GP, Isaacs MJ, Kawakami Y et al (2007) BMP-3 and BMP-6 structures illuminate the nature of binding specificity with receptors. *Biochemistry* 46:12238–12247. <https://doi.org/10.1021/bi700907k>
- Asai-Coakwell M, French CR, Berry KM et al (2007) GDF6, a novel locus for a spectrum of ocular developmental anomalies. *Am J Hum Genet* 80:306–315
- Asai-Coakwell M, French CR, Ye M et al (2009) Incomplete penetrance and phenotypic variability characterize Gdf6-attributable oculo-skeletal phenotypes. *Hum Mol Genet* 18:1110–1121. <https://doi.org/10.1093/hmg/ddp008>
- Bahamonde ME, Lyons KM (2001) BMP3: to be or not to be a BMP. *J Bone Jt Surg Am* 83:56–62
- Bajpai R, Chen DA, Rada-Iglesias A et al (2010) CHD7 cooperates with PBAF to control multipotent neural crest formation. *Nature* 463:958–962. <https://doi.org/10.1038/nature08733>
- Bakrania P, Efthymiou M, Klein JC et al (2008) Mutations in BMP4 cause eye, brain, and digit developmental anomalies: overlap between the BMP4 and hedgehog signaling pathways. *Am J Hum Genet* 82:304–319
- Bassing CH, Howe DJ, Segarini PR et al (1994) A single heteromeric receptor complex is sufficient to mediate biological effects of transforming growth factor-beta ligands. *J Biol Chem* 269:14861–14864. [https://doi.org/10.1016/S0021-9258\(17\)36543-2](https://doi.org/10.1016/S0021-9258(17)36543-2)
- Beaulieu CL, Majewski J, Schwartzentruber J et al (2014) FORGE Canada Consortium: outcomes of a 2-year national rare-disease gene-discovery project. *Am J Hum Genet* 94:809–817. <https://doi.org/10.1016/j.ajhg.2014.05.003>
- Beby F, Commeaux C, Bozon M et al (2007) New phenotype associated with an Arg116Cys mutation in the CRYAA gene: nuclear cataract, iris coloboma, and microphthalmia. *Arch Ophthalmol* 125:213–216. <https://doi.org/10.1001/archophth.125.2.213>
- Beleggia F, Li Y, Fan J et al (2015) CRIM1 haploinsufficiency causes defects in eye development in human and mouse. *Hum Mol Genet* 24:2267–2273. <https://doi.org/10.1093/hmg/ddu744>
- Bernstein CS, Anderson MT, Gohel C et al (2018) The cellular bases of choroid fissure formation and closure. *Dev Biol* 440:137–151. <https://doi.org/10.1016/j.ydbio.2018.05.010>
- Brady JP, Garland D, Duglas-Tabor Y et al (1997) Targeted disruption of the mouse α A-crystallin gene induces cataract and cytoplasmic inclusion bodies containing the small heat shock protein α B-crystallin. *Proc Natl Acad Sci* 94:884–889. <https://doi.org/10.1073/pnas.94.3.884>
- Bryan CD, Casey MA, Pfeiffer RL et al (2020) Optic cup morphogenesis requires neural crest-mediated basement membrane assembly. *Development* 147:dev181420. <https://doi.org/10.1242/dev.181420>
- Creuzet S, Vincent C, Couly G (2003) Neural crest derivatives in ocular and periocular structures. *Int J Dev Biol* 49:161–171
- Daluiski A, Engstrand T, Bahamonde ME et al (2001) Bone morphogenetic protein-3 is a negative regulator of bone density. *Nat Genet* 27:84–88. <https://doi.org/10.1038/83810>
- Dee CT, Szymoniuk CR, Mills PED, Takahashi T (2012) Defective neural crest migration revealed by a Zebrafish model of Alx1-related frontonasal dysplasia. *Hum Mol Genet* 22:239–251. <https://doi.org/10.1093/hmg/dds423>
- Eckert P, Knickmeyer MD, Heermann S (2020) In Vivo Analysis of optic fissure fusion in zebrafish: pioneer cells, basal lamina, hyaloid vessels, and how fissure fusion is affected by BMP. *Int J Mol Sci* 21:2760
- Eve AMJ, Place ES, Smith JC (2017) Comparison of Zebrafish tmem88a mutant and morpholino knockdown phenotypes. *PLoS ONE* 12:e0172227
- French CR, Erickson T, French DV et al (2009) Gdf6a is required for the initiation of dorsal–ventral retinal patterning and lens development. *Dev Biol* 333:37–47
- Gage PJ, Rhoades W, Prucka SK, Hjalt T (2005) Fate maps of neural crest and mesoderm in the mammalian eye. *Invest Ophthalmol vis Sci* 46:4200–4208. <https://doi.org/10.1167/iiov.05-0691>
- Gagnon JA, Valen E, Thyme SB et al (2014) Efficient mutagenesis by cas9 protein-mediated oligonucleotide insertion and large-scale assessment of single-guide RNAs. *PLoS ONE* 9:e98186
- Gamer LW, Nove J, Levin M, Rosen V (2005) BMP-3 is a novel inhibitor of both activin and BMP-4 signaling in *Xenopus* embryos. *Dev Biol* 285:156–168. <https://doi.org/10.1016/j.ydbio.2005.06.012>
- Gestri G, Osborne RJ, Wyatt AW et al (2009) Reduced TFAP2A function causes variable optic fissure closure and retinal defects and sensitizes eye development to mutations in other morphogenetic regulators. *Hum Genet* 126:791–803. <https://doi.org/10.1007/s00439-009-0730-x>
- Gestri G, Bazin-Lopez N, Scholes C, Wilson SW (2018) Cell behaviors during closure of the choroid fissure in the developing eye. *Front Cell Neurosci* 12:42
- Goebel EJ, Hart KN, McCoy JC, Thompson TB (2019) Structural biology of the TGF β family. *Exp Biol Med* 244:1530–1546. <https://doi.org/10.1177/1535370219880894>
- Gosse NJ, Baier H (2009) An essential role for Radar (Gdf6a) in inducing dorsal fate in the zebrafish retina. *Proc Natl Acad Sci* 106:2236–2241. <https://doi.org/10.1073/pnas.0803202106>
- Graff JM, Bansal A, Melton DA (1996) *Xenopus* mad proteins transduce distinct subsets of signals for the TGF β superfamily. *Cell* 85:479–487. [https://doi.org/10.1016/S0092-8674\(00\)81249-0](https://doi.org/10.1016/S0092-8674(00)81249-0)
- Hanel ML, Hensley C (2006) Eye and neural defects associated with loss of GDF6. *BMC Dev Biol* 6:43. <https://doi.org/10.1186/1471-213X-6-43>
- Hardy H, Prendergast JGD, Patel A et al (2019) Detailed analysis of chick optic fissure closure reveals Netrin-1 as an essential mediator of epithelial fusion. *Elife* 8:e43877

- Hero I (1989) The optic fissure in the normal and microphthalmic mouse. *Exp Eye Res* 49:229–239. [https://doi.org/10.1016/0014-4835\(89\)90093-6](https://doi.org/10.1016/0014-4835(89)90093-6)
- Hero I (1990) Optic fissure closure in the normal cinnamon mouse. An ultrastructural study. *Invest Ophthalmol vis Sci* 31:197–216
- Hornby SJ, Dandona L, Jones RB et al (2003) The familial contribution to non-syndromic ocular Coloboma in south India. *Br J Ophthalmol* 87:336–340. <https://doi.org/10.1136/bjo.87.3.336>
- Ittner LM, Wurdak H, Schwerdtfeger K et al (2005) Compound developmental eye disorders following inactivation of TGF β signaling in neural-crest stem cells. *J Biol* 4:11
- James A, Lee C, Williams AM et al (2016) The hyaloid vasculature facilitates basement membrane breakdown during choroid fissure closure in the zebrafish eye. *Dev Biol* 419:262–272. <https://doi.org/10.1016/j.ydbio.2016.09.008>
- Jinnin M, Ihn H, Tamaki K (2006) Characterization of SIS3, a novel specific inhibitor of Smad3, and its effect on transforming growth factor- β 1-induced extracellular matrix expression. *Mol Pharmacol* 69:597–607. <https://doi.org/10.1124/mol.105.017483>
- Kagiyama Y, Gotouda N, Sakagami K et al (2005) Extraocular dorsal signal affects the developmental fate of the optic vesicle and patterns the optic neuroepithelium. *Dev Growth Differ* 47:523–536. <https://doi.org/10.1111/j.1440-169X.2005.00828.x>
- Kim T-H, Goodman J, Anderson KV, Niswander L (2007) Phactr4 regulates neural tube and optic fissure closure by controlling PP1-, Rb-, and E2F1-regulated cell-cycle progression. *Dev Cell* 13:87–102. <https://doi.org/10.1016/j.devcel.2007.04.018>
- Kimmel CB, Ballard WW, Kimmel SR et al (1995) Stages of embryonic development of the zebrafish. *Dev Dyn* 203:253–310
- Kimmel CB, Miller CT, Kruze G et al (1998) The shaping of pharyngeal cartilages during early development of the zebrafish. *Dev Biol* 203:245–263. <https://doi.org/10.1006/dbio.1998.9016>
- Knickmeyer MD, Mateo JL, Eckert P et al (2020) TGF β -facilitated optic fissure fusion and the role of bone morphogenetic protein antagonism. *Open Biol* 8:170134. <https://doi.org/10.1098/rsob.170134>
- Kwan KM, Otsuna H, Kidokoro H et al (2012) A complex choreography of cell movements shapes the vertebrate eye. *Development* 139:359–372. <https://doi.org/10.1242/dev.071407>
- Langenberg T, Kahana A, Wszalek JA, Halloran MC (2008) The eye organizes neural crest cell migration. *Dev Dyn* 237:1645–1652. <https://doi.org/10.1002/dvdy.21577>
- Laurie KJ, Dave A, Straga T et al (2013) Identification of a novel oligomerization disrupting mutation in CRYAA associated with congenital cataract in a South Australian Family. *Hum Mutat* 34:435–438. <https://doi.org/10.1002/humu.22260>
- Lee J, Lee B-K, Gross JM (2013) Bcl6a function is required during optic cup formation to prevent p53-dependent apoptosis and Colobomata. *Hum Mol Genet* 22:3568–3582. <https://doi.org/10.1093/hmg/ddt211>
- Levitt M (1978) Conformational preferences of amino acids in globular proteins. *Biochemistry* 17:4277–4285. <https://doi.org/10.1021/bi00613a026>
- Litt M, Kramer P, LaMorticella DM et al (1998) Autosomal dominant congenital cataract associated with a missense mutation in the human alpha crystallin gene CRYAA. *Hum Mol Genet* 7:471–474. <https://doi.org/10.1093/hmg/7.3.471>
- Little SC, Mullins MC (2006) Extracellular modulation of BMP activity in patterning the dorsoventral axis. *Birth Defects Res Part C Embryo Today Rev* 78:224–242. <https://doi.org/10.1002/bdrc.20079>
- Liu F, Hata A, Baker JC et al (1996) A human Mad protein acting as a BMP-regulated transcriptional activator. *Nature* 381:620–623. <https://doi.org/10.1038/381620a0>
- Livak KJ, Schmittgen TD (2001) Analysis of relative gene expression data using real-time quantitative PCR and the 2 $^{-\Delta\Delta CT}$ method. *Methods* 25:402–408. <https://doi.org/10.1006/meth.2001.1262>
- Lo RS, Chen YG, Shi Y et al (1998) The L3 loop: a structural motif determining specific interactions between SMAD proteins and TGF-beta receptors. *EMBO J* 17:996–1005. <https://doi.org/10.1093/emboj/17.4.996>
- Luo R, An M, Arduini BL, Henion PD (2001) Specific pan-neural crest expression of zebrafish Crestin throughout embryonic development. *Dev Dyn* 220:169–174. [https://doi.org/10.1002/1097-0177\(2000\)9999:9999%3c::AID-DVDY1097%3e3.0.CO;2-1](https://doi.org/10.1002/1097-0177(2000)9999:9999%3c::AID-DVDY1097%3e3.0.CO;2-1)
- Lupo G, Gestri G, O'Brien M et al (2011) Retinoic acid receptor signaling regulates choroid fissure closure through independent mechanisms in the ventral optic cup and periorcular mesenchyme. *Proc Natl Acad Sci U S A* 108:8698–8703. <https://doi.org/10.1073/pnas.1103802108>
- Mackay DS, Andley UP, Shiels A (2003) Cell death triggered by a novel mutation in the alphaA-crystallin gene underlies autosomal dominant cataract linked to chromosome 21q. *Eur J Hum Genet* 11:784–793. <https://doi.org/10.1038/sj.ejhg.5201046>
- Matsuoka RL, Chivatakarn O, Badea TC et al (2011) Class 5 transmembrane semaphorins control selective mammalian retinal lamination and function. *Neuron* 71:460–473. <https://doi.org/10.1016/j.neuron.2011.06.009>
- McMahon C, Gestri G, Wilson SW, Link BA (2009) Lmx1b is essential for survival of periorcular mesenchymal cells and influences Fgf-mediated retinal patterning in zebrafish. *Dev Biol* 332:287–298. <https://doi.org/10.1016/j.ydbio.2009.05.577>
- Melo F, Devos D, Depiereux E, Feytmans E (1997) ANOLEA: a www server to assess protein structures. *Intell Syst Mol Biol* 97:110–113
- Miyashita T, Baddam P, Smeeton J et al (2020) nkx3.2 mutant zebrafish accommodate jaw joint loss through a phenocopy of the head shapes of Paleozoic jawless fish. *J Exp Biol*. <https://doi.org/10.1242/jeb.216945>
- Miyazono K, Ten Dijke P, Heldin C-H (2000) TGF- β signaling by Smad proteins. Academic Press, pp 115–157
- Morcillo J, Martínez-Morales JR, Trouse F et al (2006) Proper patterning of the optic fissure requires the sequential activity of BMP7 and SHH. *Development* 133:3179–3190. <https://doi.org/10.1242/dev.02493>
- Morrison D, FitzPatrick D, Hanson I et al (2002) National study of microphthalmia, anophthalmia, and coloboma (MAC) in Scotland: investigation of genetic aetiology. *J Med Genet* 39:16–22. <https://doi.org/10.1136/jmg.39.1.16>
- Mueller RL, Huang C, Ho RK (2010) Spatio-temporal regulation of Wnt and retinoic acid signaling by tbx16/spadetail during zebrafish mesoderm differentiation. *BMC Genom* 11:492. <https://doi.org/10.1186/1471-2164-11-492>
- Noh H, Lee H, Park E, Park S (2016) Proper closure of the optic fissure requires ephrin A5-EphB2-JNK signaling. *Development* 143:461–472. <https://doi.org/10.1242/dev.129478>
- Okada I, Hamanoue H, Terada K et al (2011) SMOC1 is essential for ocular and limb development in humans and mice. *Am J Hum Genet* 88:30–41. <https://doi.org/10.1016/j.ajhg.2010.11.012>
- Patel A, Sowden JC (2019) Genes and pathways in optic fissure closure. *Semin Cell Dev Biol* 91:55–65. <https://doi.org/10.1016/j.semcdb.2017.10.010>
- Peters MA, Cepko CL (2002) The dorsal-ventral axis of the neural retina is divided into multiple domains of restricted gene expression which exhibit features of lineage compartments. *Dev Biol* 251:59–73. <https://doi.org/10.1006/dbio.2002.0791>
- Pfirrmann T, Emmerich D, Ruokonen P et al (2015) Molecular mechanism of CHRDL1-mediated X-linked megalocornea in humans and in Xenopus model. *Hum Mol Genet* 24:3119–3132. <https://doi.org/10.1093/hmg/ddv063>

- Pillay LM, Forrester AM, Erickson T et al (2010) The Hox cofactors Meis1 and Pbx act upstream of gata1 to regulate primitive hematopoiesis. *Dev Biol* 340:306–317. <https://doi.org/10.1016/j.ydbio.2010.01.033>
- Pras E, Frydman M, Levy-Nissenbaum E et al (2000) A nonsense mutation (W9X) in CRYAA causes autosomal recessive cataract in an inbred Jewish Persian Family. *Invest Ophthalmol vis Sci* 41:3511–3515
- Prince VE, Moens CB, Kimmel CB, Ho RK (1998) Zebrafish hox genes: expression in the hindbrain region of wild-type and mutants of the segmentation gene, valentino. *Development* 125:393–406
- Prokudin I, Simons C, Grigg JR et al (2014) Exome sequencing in developmental eye disease leads to identification of causal variants in GJA8, CRYGC, PAX6 and CYP1B1. *Eur J Hum Genet* 22:907–915. <https://doi.org/10.1038/ejhg.2013.268>
- Reis LM, Tyler RC, Schilter KF et al (2011) BMP4 loss-of-function mutations in developmental eye disorders including SHORT syndrome. *Hum Genet* 130:495–504. <https://doi.org/10.1007/s00439-011-0968-y>
- Richter L, Flodman P, Barria-von-Bischhoffshausen F et al (2008) Clinical variability of autosomal dominant cataract, microcornea and corneal opacity and novel mutation in the alpha A crystallin gene (CRYAA). *Am J Med Genet Part A* 146A:833–842. <https://doi.org/10.1002/ajmg.a.32236>
- Rochard L, Monica SD, Ling ITC et al (2016) Roles of Wnt pathway genes wls, wnt9a, wnt5b, frzb and gpc4 in regulating convergent-extension during zebrafish palate morphogenesis. *Development* 143:2541–2547. <https://doi.org/10.1242/dev.137000>
- Sakuta H, Suzuki R, Takahashi H et al (2001) Ventroptin: a BMP-4 antagonist expressed in a double-gradient pattern in the retina. *Science* 293:111–115. <https://doi.org/10.1126/science.1058379>
- Schmitt EA, Dowling JE (1994) Early-eye morphogenesis in the zebrafish, *Brachydanio rerio*. *J Comp Neurol* 344:532–542. <https://doi.org/10.1002/cne.903440404>
- Schoenebeck JJ, Hutchinson SA, Byers A et al (2012) Variation of BMP3 contributes to dog breed skull diversity. *PLOS Genet* 8:e1002849
- Sedykh I, Yoon B, Roberson L et al (2017) Zebrafish zic2 controls formation of periocular neural crest and choroid fissure morphogenesis. *Dev Biol* 429:92–104. <https://doi.org/10.1016/j.ydbio.2017.07.003>
- Sghari S, Gunhaga L (2018) Temporal requirement of Mab21l2 during eye development in chick reveals stage-dependent functions for retinogenesis. *Invest Ophthalmol vis Sci* 59:3869–3878. <https://doi.org/10.1167/iovs.18-24236>
- Shah SP, Taylor AE, Sowden JC et al (2012) Anophthalmos, microphthalmos, and coloboma in the United Kingdom: clinical features, results of investigations, and early management. *Ophthalmology* 119:362–368. <https://doi.org/10.1016/j.ophtha.2011.07.039>
- Siebert JR, Graham JM Jr, MacDonald C (1985) Pathologic features of the CHARGE association: support for involvement of the neural crest. *Teratology* 31:331–336
- Skarie JM, Link BA (2009) FoxC1 is essential for vascular basement membrane integrity and hyaloid vessel morphogenesis. *Invest Ophthalmol vis Sci* 50:5026–5034. <https://doi.org/10.1167/iovs.09-3447>
- Stewart A, Guan H, Yang K (2010) BMP-3 promotes mesenchymal stem cell proliferation through the TGF- β /activin signaling pathway. *J Cell Physiol* 223:658–666. <https://doi.org/10.1002/jcp.22064>
- Sun Z, Zhou Q, Li H et al (2017) Mutations in crystallin genes result in congenital cataract associated with other ocular abnormalities. *Mol vis* 23:977–986
- Suzuki S, Marazita ML, Cooper ME et al (2009) Mutations in BMP4 are associated with subepithelial, microform, and overt cleft lip. *Am J Hum Genet* 84:406–411. <https://doi.org/10.1016/j.ajhg.2009.02.002>
- Takamiya M, Stegmaier J, Kobitski AY et al (2020) Pax6 organizes the anterior eye segment by guiding two distinct neural crest waves. *PLoS Genet*. <https://doi.org/10.1371/journal.pgen.1008774>
- Thisse C, Thisse B (2008) High-resolution in situ hybridization to whole-mount zebrafish embryos. *Nat Protoc* 3:59–69. <https://doi.org/10.1038/nprot.2007.514>
- Trost A, Schroedl F, Lange S et al (2013) Neural crest origin of retinal and choroidal pericytes. *Invest Ophthalmol vis Sci* 54:7910–7921. <https://doi.org/10.1167/iovs.13-12946>
- Tsuji N, Kita K, Ozaki K et al (2012) Organogenesis of mild ocular coloboma in FLS mice: failure of basement membrane disintegration at optic fissure margins. *Exp Eye Res* 94:174–178. <https://doi.org/10.1016/j.exer.2011.12.004>
- Van Nostrand JL, Brady CA, Jung H et al (2014) Inappropriate p53 activation during development induces features of CHARGE syndrome. *Nature* 514:228–232. <https://doi.org/10.1038/nature13585>
- Viringipurampeer IA, Ferreira T, DeMaria S et al (2012) Pax2 regulates a fadd-dependent molecular switch that drives tissue fusion during eye development. *Hum Mol Genet* 21:2357–2369. <https://doi.org/10.1093/hmg/dds056>
- Walker M, Kimmel C (2007) A two-color acid-free cartilage and bone stain for zebrafish larvae. *Biotech Histochem* 82:23–28. <https://doi.org/10.1080/10520290701333558>
- Williamson KA, FitzPatrick DR (2014) The genetic architecture of microphthalmia, anophthalmia and coloboma. *Eur J Med Genet* 57:369–380. <https://doi.org/10.1016/j.ejmg.2014.05.002>
- Wrana JL, Attisano L, Cárcamo J et al (1992) TGF- β signals through a heteromeric protein kinase receptor complex. *Cell* 71:1003–1014. [https://doi.org/10.1016/0092-8674\(92\)90395-S](https://doi.org/10.1016/0092-8674(92)90395-S)
- Wyatt AW, Osborne RJ, Stewart H, Ragge NK (2010) Bone morphogenetic protein 7 (BMP7) mutations are associated with variable ocular, brain, ear, palate, and skeletal anomalies. *Hum Mutat* 31:781–787. <https://doi.org/10.1002/humu.21280>
- Yan X, Atorf J, Ramos D et al (2020) Mutation in Bmpr1b leads to optic disc coloboma and ventral retinal gliosis in mice. *Invest Ophthalmol vis Sci* 61:44. <https://doi.org/10.1167/iovs.61.2.44>
- Ye M, Berry-Wynne KM, Asai-Coakwell M et al (2010) Mutation of the bone morphogenetic protein GDF3 causes ocular and skeletal anomalies. *Hum Mol Genet* 19:287–298. <https://doi.org/10.1093/hmg/ddp496>
- Yoon KH, Fox SC, Dicipulo R et al (2020) Ocular coloboma: genetic variants reveal a dynamic model of eye development. *Am J Med Genet Part C Semin Med Genet* 184C:590–610. <https://doi.org/10.1002/ajmg.c.31831>
- Zhang Y, Feng X-H, Wu R-Y, Derynck R (1996) Receptor-associated Mad homologues synergize as effectors of the TGF- β response. *Nature* 383:168–172. <https://doi.org/10.1038/383168a0>
- Zhang R, Huang H, Cao P et al (2013) Sma- and Mad-related protein 7 (Smad7) is required for embryonic eye development in the mouse. *J Biol Chem* 288:10275–10285. <https://doi.org/10.1074/jbc.M112.416719>
- Zuber ME, Gestri G, Viczian AS et al (2003) Specification of the vertebrate eye by a network of eye field transcription factors. *Development* 130:5155–5167